Cytochrome P450 2E1/Nickel-Poly(propylene imine) Dendrimeric Nanobiosensor for Pyrazinamide - A First Line TB Drug

UNIVERSITY *of the*
WESTERN CAPE

By

Mlandeli Siphelele Ernest Zosiwe
(BSc Honours)

A mini-thesis submitted in partial fulfilment of the requirements for the degree of

Magister Scientiae in Nanoscience

Faculty of Science

University of the Western Cape

Bellville, Cape Town, South Africa

Supervisor: Prof Emmanuel I. Iwuoha

July, 2015

Keywords

Pyrazinamide drug

Cytochrome P450 2E1 (CYP2E1)

Conducting star copolymers

Metallodendrimers

Biosensors

Cyclic voltammetry

Limit of detection (LOD)

Nickel poly(propylene imine)–co-polypyrrole (Ni-PPI-Ppy) star copolymer

ABSTRACT

The tuberculosis (TB) disease to this day remains one of the world's prominent killer diseases. Pyrazinamide (PZA) is one of the most commonly prescribed anti-tuberculosis (anti-TB) drugs due to its ability to significantly shorten the TB treatment period from the former nine months to the current six months duration. However, excess PZA in the body causes hepatotoxicity and damages the liver. This hepatotoxicity, together with the resistance of the bacteria to treatment drugs, poor medication and inappropriate dosing, greatly contribute to the high incidents of TB deaths and diseases that are due to side effects (such as liver damage). This brings about the calls for alternative methods for ensuring reliable dosing of the drug, which will be specific from person to person due to inter-individual differences in drug metabolism. A novel biosensor system for monitoring the metabolism of PZA was prepared with a Ni-PPI-PPy star copolymer and cytochrome P450 2E1 (CYP2E1) deposited onto a platinum electrode. The nanobiosensor system exhibited enhanced electro-activity that is attributed to the catalytic effect of the incorporated star copolymer. The biosensor had a sensitivity of 0.142 $\mu A.nM^{-1}$, and a dynamic linear range (DLR) of 0.01 nM-0.12 nM (1.231 – 7.386 ng/L PZA). The limit of detection of the biosensor was found to be 0.00114 nM (0.14 ng/L) PZA. From the HPLC peak concentration (C_{max}) of PZA determined 2 h after drug intake is 2.79 – 3.22 $ng.L^{-1}$, which is very detectable with the nanobiosensor as it falls within the dynamic linear range.

Declaration

I declare that "Cytochrome P450 2E1/Nickel-Poly(propylene imine) Dendrimeric Nanobiosensor for Pyrazinamide - A First Line TB Drug*''* is my own work, that it has not been submitted before for any degree or examination in any other university, and that all the sources I have used or quoted have been indicated or acknowledged as complete references.

Mlandeli Siphelele Ernest Zosiwe November 2014

Signed ……

Acknowledgements

I would like to thank God for giving me the strength to complete my work.

A special thanks to my supervisor, Prof Emmanuel Iwuoha, for his guidance, support and for believing in me throughout the study. To Dr. Abd. Baleg and Dr. R.F Ajayi thank you for your support. To all family and friends, I am grateful for your love, motivation and support throughout the period of the study.

To all my Seniors and colleagues: Xolani Simelane, Wonderboy Hlongwa, Myra Nzaba, Lerato Nkuna, Nomxolisi Dywili, Lindsay Wilson, Meryck Ward, Francis Muya, Masikini Milua and Candice Rassie. Thank you for your co-operation and assistance during my studies in the Sensorlab.

To Nomaphelo Ntshongontshi: Thank you for playing a very important role in both my academic and personal life. I highly appreciate you and everyday spent with you. If it were not for your support and motivation, I wouldn't be where I am today. Thank you, dear Sister.

To the Chemistry Department staff and Sensorlab researchers, thank you for your friendship and support. Last but certainly not least, I would like to thank the Department of Science and Technology for the funding to undertake this study.

Dedication

This work is dedicated to: my mother Beauty Bulelwa Zosiwe and my siblings Lizo Siviwe Oscar Zosiwe and Xolani Gcolotela.

Contents

List of abbreviations

Abbreviation	Definition
PPI	poly(propylene imine)
PPy	Polypyrrole
Ni	Nickel
TB	Tuberculosis
WHO	World Health Organization
CYP2E1	Cytochrome P450-2E1 enzyme
PBS	Phosphate buffer solution
Pt	Platinum electrode
FTIR Fourier	Fourier Transformation Infrared spectroscopy
CV	Cyclic voltammetry
EDS	Energy dispersive spectrometry (spectroscopy)
HRSEM	High resolution scanning electron microscopy
HRTEM	High resolution transmission electron microscopy
G2	Generation 2

Ni-PPI-PPY	Nickel generation-2 poly(propylene imine)-co-polypyrrole star copolymer
Ni-PPI-Py	Nickel generation-2 poly(propylene imine)-2 Pyrrole
PPI-2Py	Generation 2 poly(propylene imine)-2Pyrrole
DLR	Dynamic linear range
LOD	Limit of detection
PZA	Pyrazinamide
D_o	Diffusion co-efficient
E_{pc}	Cathodic peak potential
E_{pa}	Anodic peak potential
C_{max}	Highest observed plasma concentration
E^0	Formal potential

List of figures

Figure 17: Cyclic Voltammogram of Ni-PPI-Ppy/CYP2E1/BSA/Glu/Pt with different concentrations of PZA in 0.1 phosphate buffer taken from -800 to -100 mV (vs. Ag/AgCl).

Figure 18: Calibration curve drawn from the linear region of the biosensor responses in figure 16.

CHAPTER 1

INTRODUCTION

Summary

This chapter describes the aspects involved in the study namely; Dendrimers, sensors, cytochrome P450 enzymes (with particular emphasis on CYP450 2E1), tuberculosis, and anti-tuberculosis treatment drugs in which the study will focus on pyrazinamide as a model drug. The focus of this chapter is the relationship between all of these aspects and the manner in which they contribute towards the success and applicability of this study. The chapter also includes the problem statement, motivation, aim and objectives of the study as well as the thesis outline.

1.1. Background

Tuberculosis (TB) is an infectious disease that is caused by the bacteria bacillus Mycobacterium tuberculosis. TB classically affects the lungs (pulmonary TB) but can affect other sites as well (extrapulmonary TB). TB spreads in the air when people who are infected with the pulmonary TB eject the bacteria, by coughing as an example. TB remains one of the world's deadliest communicable diseases. In 2013, an estimated 9.0 million people developed TB and 1.5 million died from the disease, 360 000 of whom were HIV-positive **[1].** Mycobacterial infections are one of the most difficult bacterial infections to treat, let alone cure. This is because mycobacteria are organisms that grow at a slow rate, which makes them relatively resistant to antibiotics, an activity of which tends to depend on how rapidly the cells are dividing **[2].** Most people who are exposed to TB

never develop symptoms because the bacteria can live in an inactive form in the body for years without being activated. Due to the fact that these latent infections can ultimately become active, even people who show no symptoms should receive medical treatment. In such cases, the therapy gets rid of the inactive bacteria before they become active. Inactive mycobacterial cells can be completely resistant to many drugs, or at times be slowly killed by drugs that are active **[1]**. When the immune system weakens, such as in people who are infected with the HIV or elderly persons, the bacteria can be activated. In their active state, TB bacteria cause death to the tissue of the infected organs. Active TB disease can be fatal if it is left untreated. A considerable amount of mycobacterial cells are intracellular, they reside inside macrophages which makes them practically unreachable to drugs that struggle to infiltrate the macrophages **[1]**. These organisms, infamous for developing resistance to any single drug, therefore, require a combination drug therapy to successfully overcome such obstacles and also prevent the development of resistance during therapy. Another alternative approach to eliminating mycobacteria is chemotherapy. The drawback of this approach is that it is a slow means of therapy whereby treatment can drag on for months to years, depending on the drugs used **[2]**.

Tuberculosis is one of the main subjects of this study, and is a disease resulting from infection, primarily, by *Mycobacterium tuberculosis* which is the most prominent infecting organism. There are, on the other hand, other rare mycobacteria that can give rise to the development of TB such as *Mycobacterium bovis,* which is infrequent because of the practical eradication of bovine tuberculosis from cattle as well as *Mycobacterium africanum,* which is usually found in parts of Africa **[2]**.

There exists a clear difference between tuberculosis infection and tuberculosis disease. In the case of tuberculosis disease, one or more body parts show bacteriological, clinical and radiographic evidence of the disease while in the case of tuberculosis infection; the tubercle bacilli are established in the host with no symptoms or detectable evidence of the disease. During the last few decades, TB infections and fatality rate has decreased gradually **[3]**. This could be attributed to a combination of improved social conditions, better nutrition, less overcrowding, freely available vaccination and case-finding programmes **[2].** There has been a global decrease in new TB cases since 2003, but despite that, developing counties in Africa are still feeling the effects of the disease. In 2006 South Africa recorded the world's second highest rate of new cases after Swaziland **[1]**. More people died of TB in South Africa in that year than in any other country in the world, at a rate of 218 per 100 000. Zimbabwe and Mozambique had the next highest TB death rates. The global TB cure rate for 2005 was 78%, but South Africa's cure rate was only 58%. This was third worst in the world. Uganda was bottom of the class with a 32% cure rate, followed by Russia with a 55% cure rate. Zimbabwe did marginally better than South Africa with a 59% cure rate. In underdeveloped and developing countries, TB continues to be problematic especially with the emergence of drug resistant strains and the high rates of HIV/AIDS **[3]**.

The most recent global TB estimates show that 9 million people developed TB in 2013 and 1.5 million fatalities resulted from the disease **[1]**. Of the estimated 9 million people who developed TB in 2013, more than half (56%) were in the South-East Asia and

Western Pacific Regions. A further one quarter was in the African Region, which also had the highest rates of new cases and deaths relative to population **[3].** The persistence of high infection rates in these countries can be accredited to the lack of proper public infrastructure and the accelerated weakening of the immune system of the individuals who are infected with the HIV/AIDS.

The directly observed treatment short course (DOTS) regime has played a key and significant role in reducing the infection and death rates of TB. However, failure to complete the treatment as well as inappropriate dosing, have also been a major cause of the high occurrences of the drug resistant strains of TB **[2]**. The spread of HIV/AIDS in tuberculosis-endemic regions also plays a role in the development of the TB drug resistant strains. This is due to the fact that patients with fully susceptible tuberculosis develop secondary resistance during therapy, resulting from inappropriate dosing of treatment drugs, inadequate treatment, not taking the prescribed regimen appropriately or using low quality medication **[2]**. Multidrug-resistant TB (MDR-TB) and extensively drug resistant TB (XRD-TB) are both the TB drug resistant strains which are more difficult to treat than sensitive tuberculosis, since they require the administration of expensive and less effective second line drugs for longer treatment durations than first line drugs **[1,2]**. This highlights the need for new approaches to remedy the situation of patients becoming sick because of inappropriate dosing and inadequate administration of the treatment drugs.

In order for that to be achieved, a device that has a fast response time together with an enhanced performance and increased sensitivity is fundamental. This type of a device can only become a possibility by adopting the lab-on-a-chip principle, which is obtained by

the reducing the size of bulky lab equipment and integrating them onto a single chip. The size reduction is paramount because it brings about ease of convenience, portability, low costs, high resolution results, ease of operation, rapidity of analysis and reduced amounts of chemical or sample consumption **[4]**. Amongst the methods currently used for miniaturization is the integration of chemical techniques and procedures into electrochemical nanobiosensors. An electrochemical nanobiosensor consists of two parts, one where the requisite chemical or physical processes are performed and the second part for the acquirement of information **[3]**. Nanobiosensors require a biological element such as DNA or enzymes to be integrated into the sensing material **[5, 6]**. These biological elements are responsible for the determination of the analyte. The transducer component of the biosensor works physic.-chemically; it can either be optical, piezoelectric or electrochemical. The role of the transducer component is to transform the resultant signal from the sensitive biological element and analyte into another signal that is easily measured, quantified and interpreted **[3]**. Transducer elements in electrochemical biosensors, modified electrodes are often used as transducer elements, these electrodes can be coated with electric conducting substances such as quantum dots and conducting polymers, amongst others **[7]**. Conducting polymers are nanomaterials that have a large surface area and catalytic behaviour which gives them enhanced performance and properties **[8]**. Literature has revealed that incorporation of metal nanoparticles onto polymers results in nanocomposites of enhanced electrochemical activity, thereby yielding biosensors with high selectivity, sensitivity and faster response times **[3]**.

1.2. Problem statement and motivation

Pyrazinamide (PZA) is a first line pro-drug in the TB combination chemotherapy where it is administered in conjunction with rifampicin, ethambutol and isoniazid. PZA **(Figure 1)** is very active against the old bacilli of mycobacterium tuberculosis that duplicate slowly and cannot be killed by the other anti-tuberculosis drugs **[2]**. People do not metabolize drugs at the same rate and are categorized into three classes according to the rate at which they metabolize drugs, namely slow, moderate and fast metabolizers. The medical prescription assumes that everyone is a moderate metabolizer since the metabolic profile of patients is not known. This leads to greater chances of liver damage and hepatotoxicity induced by the accumulation of the drug and/or its metabolites. As a result, regulatory bodies such as FDA and WHO have set minimal inhibitory concentrations (MIC) for therapeutic drugs, with an MIC of 50–100 mg/L for PZA **[1, 9-10]** reports from bodies implemented to monitor TB (e.g. the DOTS, STOP-TB and TAC), have shown success in combating TB spread and recurrence, tuberculosis remains a major health problem in South Africa. This is enhanced by factors such as over-crowding (since TB is a respiratory disease spread easily through coughing and breathing), and poor health seeking behaviour (mainly in rural areas which constitute larger population percentages), leading to delayed detection of diseases. Above all, the TB-HIV correlation plays a vital part with 73% of TB patients being HIV positive **[1]**. Also, a recent report has confirmed that PZA metabolites are responsible for hepatotoxicity **[3]**. Hence, there is an increased demand for onsite analytical devices that can quantitatively and qualitatively allow monitoring of PZA (and other therapeutic drugs) with high sensitivity, selectivity and faster response time and lower detection limits **[9]**.

In this study we employed a conducting polymer to promoter electron transfer, conducting polymers are organic materials that exhibit both metallic and semi-conductive nature and have a conjugation of σ electrons (single bonds) and π (double bonds) along their backbone. Conducting polymers have been used as biosensor platforms due to alternating single and double bonds in the polymer chain, this special conjugation along their chain enables them to de-localize the electrons throughout the whole system resulting in them being shared by many atoms.

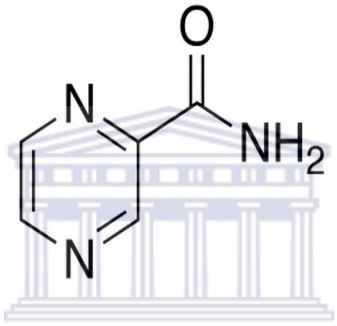

Figure 1: Structure of pyrazinamide **[10]**.

1.3. Aims and Objectives

The main aim of this study was to prepare a nanobiosensor system for monitoring the metabolism of the anti-TB drug, pyrazinamide. The platform of the biosensor consisted of a nickel-poly(propylene imine)-co-polypyrrole dendrimeric star copolymer and CYP2E1 enzyme. The enzyme was employed to act as the receptor of the sensor which will interact with the drugs while the dendrimeric star copolymer will promote electron transfer between the enzyme and the electrode.

In this research study a quantitative research approach was applied and the aim was achieved through the following objectives:

- Synthesis of G2 PPI-2Py.
- Synthesis of nickel-poly(propylene imine) (Ni-PPI-2Py) metallodendrimer.
- Fourier Transform Infrared Radiation Spectroscopic characterization of Ni-PPI-2Py metallodendrimer.
- Microscopic analysis of the of Ni-PPI-2Py metallodendrimer.
- Electropolymerization of Ni-PPI-2Py modified Pt electrode to form Ni-PPI-PPY star copolymer.
- Electroanalysis of the Ni-PPI-PPY star copolymer-modified Pt using cyclic voltammetry (CV).
- Incorporation of CYP2E1 onto the Ni-PPI-PPY star copolymer modified Pt electrode resulting in Pt/Ni-PPI-PPY star copolymer/ CYP2E1 biosensor
- Electrochemical testing of the Pt/Ni-PPI-PPY star copolymer/ CYP2E1 biosensor response in the presence and absence of pyrazinamide using CV.

1.4. Thesis layout

This thesis is presented in 6 chapters

Chapter 1: Gives brief background information on the project, problem statement and motivation as well as aims and objectives.

Chapter 2: Provides a detailed literature review.

Chapter 3: Consists of reagents, procedures and instrumentations used for the success of this study.

Chapter 4: Provides the characterization of the PPI-2Py dendrimer, Ni-PPI-2Py metallodendrimer and the developed Pt/Ni-PPI-PPY star copolymer/ CYP2E1 biosensor. Importantly it also covers results and discussion for PZA detection.

Chapter 5: Provides the conclusion and recommendations.

Chapter 6: Provides references.

CHAPTER 2

LITERATURE REVIEW

Summary

This chapter gives an introduction to electrochemical biosensors, components of an electrochemical biosensor and types of interactions involved in biosensors. This chapter also includes an introduction to conducting polymers, dendrimers and the synthesis of dendrimers.

2.1. Electroanalytical techniques

Electroanalytical techniques are concerned with the relationship between electricity and chemistry, specifically the measurement of electrical quantities such as current, potential or charge and their relationship to chemical parameters such as concentration. The use of electrical measurements for analytical purposes has found consideration in a large range of applications including environmental monitoring, industrial quality control and biomedical analysis. Amongst the devices that make use of electroanalytical techniques, biosensors are the most recently studied for quantitative and qualitative detection of various species such as drugs and hazardous chemicals, due to the negative impacts they pose on human health through their side effects. Biosensors have been getting much attention due to their properties such as portability, low cost and lower detection limits**.** These properties give biosensors application in a wide range of fields. This chapter gives an introduction to conducting polymers, their properties and their application in the field of biosensors. This chapter also gives a detailed background on different types of biosensors, the different components of a biosensor, the Cytochrome P450 enzyme family (the enzyme used in this study is CYP2E1) and tuberculosis.

2.2. Electrochemical biosensors

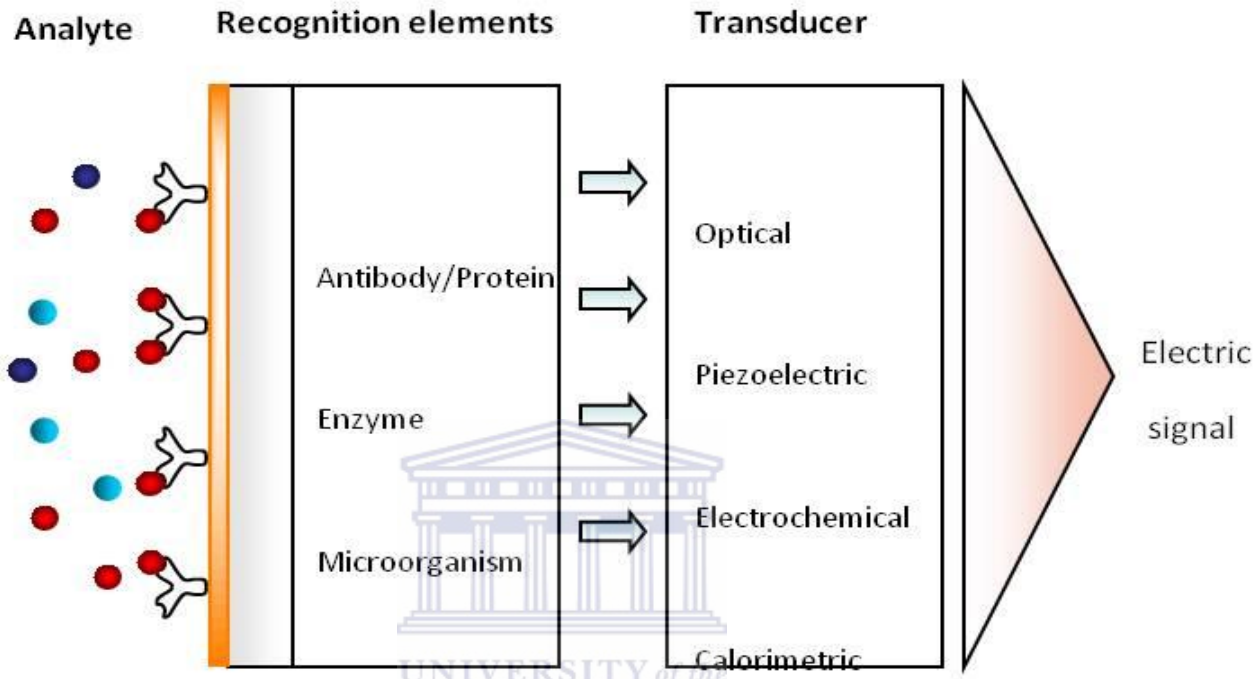

Figure 2: The components of a biosensor **[11]**.

A biosensor is an analytical device which combines a biological component with a physicochemical detector to detect an analyte **[11, 12-14]**. A biosensor consists of three components, namely, the sensitive biological element, the transducer and the signal processor. The sensitive biological element is a biologically derived material such as an enzyme, nucleic acid or a synthetic component that mimics a biological component **[12, 15]**. This biological element interacts with the analyte under study by recognizing and binding onto it **[7, 8]**.

The transducer component of the biosensor works physico-chemically; it can either be optical, piezoelectric or electrochemical. The role of the transducer component is to transform the resultant signal from the sensitive biological element and analyte into another signal that is easily measured, quantified and interpreted **[12, 16]**.

The biosensor signal processors are principally responsible for the display of the results in a convenient manner. This is typically the most expensive part of the sensor device.

2.2.1. Types of bioreceptors

Biosensor operations are dependent on the details of the sensor design. Biosensors make use of different biological and transduction elements; these can be grouped according to either of the two elements.

2.2.1.1. Antibody/antigen Interactions

An immunosensor exploits the very specific binding affinity of antibodies for an antigen. The specific nature of the antibody-antigen interaction is comparable to that of a lock and key fit in the sense that the antigen will only bind to the antibody if, and only if, it has the correct conformation **[12]**. Binding events result in a physicochemical change that, in combination with a tracer such as fluorescent molecules, enzymes or radioisotopes, can generate a signal. However, there are limitations with using antibodies in sensors. Firstly, the antibody binding capacity is strongly dependent on assay conditions (e.g. pH and temperature) and secondly, the antibody-antigen interaction is generally irreversible. However, it has been shown that binding can be disrupted by chaotropic reagents, organic solvents, or even ultrasonic radiation **[17]**.

2.2.1.2. Enzymatic Interactions

The specific binding abilities and catalytic activity of enzymes make them popular bioreceptors . Analyte recognition is allowed through several possible mechanisms such as: 1) the enzyme converting the analyte into a product that is sensor-detectable, 2) detecting enzyme inhibition or activation by the analyte, or 3) monitoring modification of enzyme properties resulting from interaction with the analyte **[18]**. The main reasons for the common use of enzymes in biosensors are: 1) ability to catalyze a large number of reactions; 2) potential to detect a group of analytes (substrates, products, inhibitors, and modulators of the catalytic activity); and 3) suitability with several different transduction methods for detecting the analyte. The major advantages of using enzymes as the receptors are that, since enzymes are not consumed in reactions, the biosensor can easily be used continuously, and that the catalytic activity of enzymes also allows lower limits of detection compared to common binding techniques. However, the sensor's lifetime is limited by the stability of the enzyme **[19]**.

2.2.1.3. Nucleic acid Interactions

Biosensors that employ nucleic acid interactions can be referred to as genosensors. The recognition process is based on the principle of complementary base pairing of adenine with thymine and cytosine with guanine in DNA. If the target nucleic acid sequence is known, complementary sequences can be synthesized, labelled and then, be immobilized on the sensor **[19]**. The hybridization probes can then base pair with the target sequences, generating an optical signal. The favoured transduction principle employed in this type of sensor has been optical detection **[12]**.

2.2.2. Types of transducer elements

2.2.2.1. Resonance

In this type of a biosensor, an acoustic wave transducer is attached to an antibody. When the analyte molecule (antigen) gets attached to the membrane, the mass of the membrane changes. The resultant change in mass subsequently changes the resonant frequency of the transducer. This frequency change is then measured **[12]**.

2.2.2.2. Optical

In this type of a biosensor, measured light is the output transduced signal. The biosensor can be made based on either optical diffraction or electrochemiluminescence. In optical diffraction-based devices, a silicon wafer is coated with a protein via covalent bonds. The wafer is then exposed to UV light through a photo-mask and the antibodies become inactive in the exposed regions. When the diced wafer chips are incubated in an analyte, antigen-antibody bindings are formed in the active regions, thus creating a diffraction grating. This grating produces a diffraction signal when illuminated with a light source such as a laser. The resulting signal can be measured or can be further amplified before measuring for improved sensitivity **[12]**.

2.2.2.3. Thermal

This type of a biosensor makes use of one of the primary properties of biological reactions, namely absorption or production of heat, which in turn changes the temperature of the medium in which the reaction takes place. They are constructed by combining

immobilized enzyme molecules with temperature sensors. When the analyte comes in contact with the enzyme, the heat reaction of the enzyme is measured and is calibrated against the analyte concentration. The total heat produced or absorbed is proportional to the molar enthalpy and the total number of molecules in the reaction. The measurement of the temperature is typically accomplished via a thermistor, and such devices are known as enzyme thermistors. Their high sensitivity to thermal changes makes thermistors ideal for such applications. Unlike other transducers, thermal biosensors do not need frequent recalibration and are insensitive to the optical and electrochemical properties of the sample. Common applications of this type of biosensor include the detection of pesticides and pathogenic bacteria **[13]**.

2.2.2.4. Ion-Sensitive

Ion-sensitive biosensors are field effect transistors (FETs) with an ion-sensitive surface. The electrical potential of the surface changes when the ions and the semiconductor interact with each other. The change in potential can then be measured. The ion-sensitive field effect transistors (ISFET) can be constructed by covering the sensor electrode with polymer layer that is selectively permeable to the analyte ions. Once the ions diffuse through the polymer layer, they bring about a change in the surface potential of the FET. This type of biosensor is sometimes referred to as enzyme field effect transistor (ENFET) and is mainly used to monitor pH **[13]**.

2.3. Conducting polymers

Conducting polymers are organic materials that exhibit both metallic and semi-conductive nature and have a conjugation of σ electrons (single bonds) and π electrons (double bonds) along their backbone Polymers were viewed as insulating materials before the 1970's **[12, 13]**. A key discovery in the research of conducting polymers was made in 1977 by McDiarmid and his colleagues when they applied to polyaniline, which is a fundamentally insulating polymer, the same redox chemistry that was previously used by both D.E Weiss *and* Gill. From this it was discovered that the conductivity of polyaniline can be increased by exposing it to either oxidizing or reducing agents **[13, 14]**.

Conductive polymers are also called conjugated polymers because of the alternating single and double bonds in the polymer chain. Due to the special conjugation in their chains, they are able to de-localize the electrons throughout the whole system resulting in their sharing by many atoms **[20]**. The de-localized electrons may move around the whole system and become the charge carriers to make polymers conductive. Non-conductive polymers can be transformed into conducting forms through the removal of electrons from the backbone (resulting in cations) or alternatively, by addition of electrons to the backbone (resulting in anions). These anions and cations act as charge carriers, hopping from one site to another under the influence of an electrical field, thus increasing conductivity of the polymer **[20]**. The single and double bond conjugation possessed by conducting polymers gives them unusual properties such as electrical conductivity, low energy optical transitions, low ionization potential and high electron affinity. The higher

values of the electrical conductivity obtained in such organic polymers have led to the name ‘synthetic metals’ **[12, 15]**.

Nanocomposites and co-polymers have emerged as the better material for biosensor due to the fact that mechanical and chemical properties of conducting polymers can be improved by doping (electron addition) or de-doping (electron removal). Copolymers synthesized from the polypropylene imine dendrimers are currently under extensive research, academically, because of their properties which will be discussed in the following section.

2.4. Dendrimers

Dendrimers are bulky and complex molecules with very distinct chemical structures. They are almost perfectly monodispersed macromolecules (since they have a consistent size and form) that can exhibit a normal and highly branched three-dimensional structure **[16]**. Dendrimers have a spherical configuration with monomer units branching out from a central core. The structure is highly defined and organized. There are two general methods to synthesizing dendrimers, namely, the divergent and the convergent methods. There is a basic difference between these two approaches. In the divergent method, scheme 1, the dendrimer grows outwards from a multifunctional core molecule. To generate the first generation dendrimer molecule, the core molecule reacts with monomer molecules containing one reactive group and two inactive groups. The generated new edge of the molecule is then activated for further reactions with more monomers. This process is then repeated for numerous generations to build the dendrimer layer by layer **[17]**.

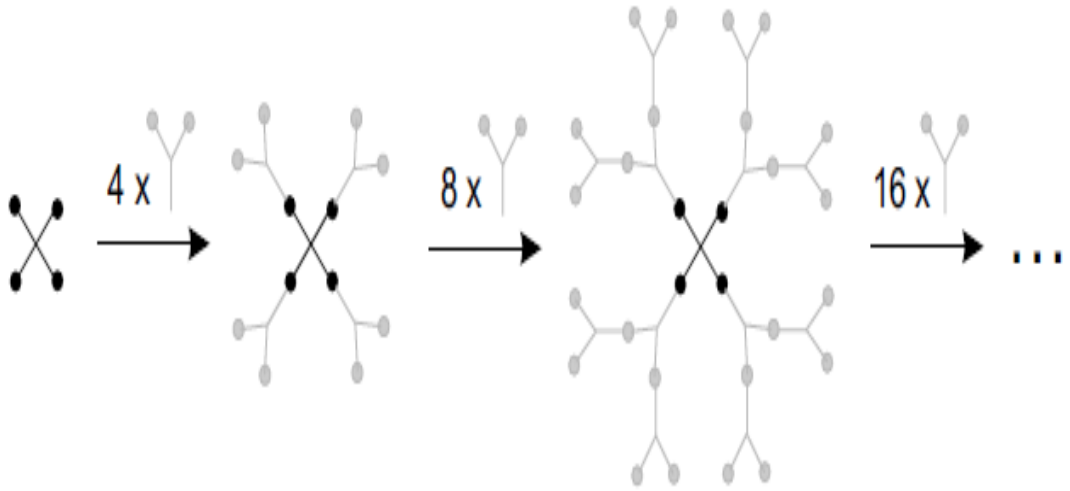

Scheme 1: The divergent method of synthesizing dendrimers.

The divergent method (**Scheme 1**) works well when producing large amounts of dendrimers, but it has problems that occur from both side and incomplete reactions of the terminal groups that bring about structural defects. To remedy both of these problems, large excess of reactants is essential, even though it brings difficulties when purifying the final product **[12]**.

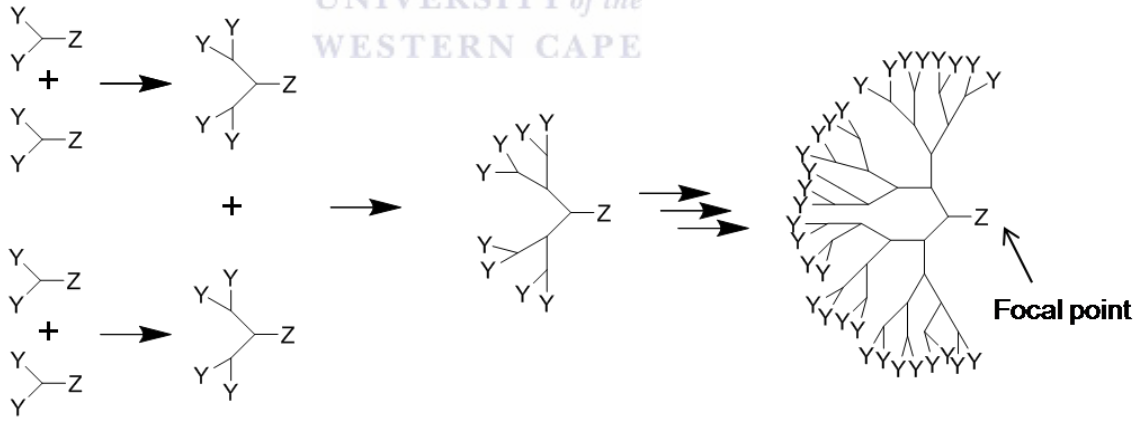

Scheme 2: The convergent method of synthesizing dendrimers **[12]**.

In the convergent method (**Scheme 2**), the dendrimer is constructed stepwise, starting from the end groups and progressing inwards. When the growing branched polymeric

arms (also called dendrons) are large enough, they are attached to a multifunctional core molecule. The convergent growth approach has quite a few advantages. Using this approach, it is relatively easy to purify the desired product and the occurrence of defects in the final structure is minimized. It becomes possible to introduce subtle engineering into the dendritic structure by precise placement of functional groups at the periphery of the macromolecule **[18, 19].** The convergent approach does not allow the formation of high generations because steric problems occur in the reactions of the dendrons and the core molecule **[21]**.

2.4.1. Poly(propylene imine) (PPI) dendrimer

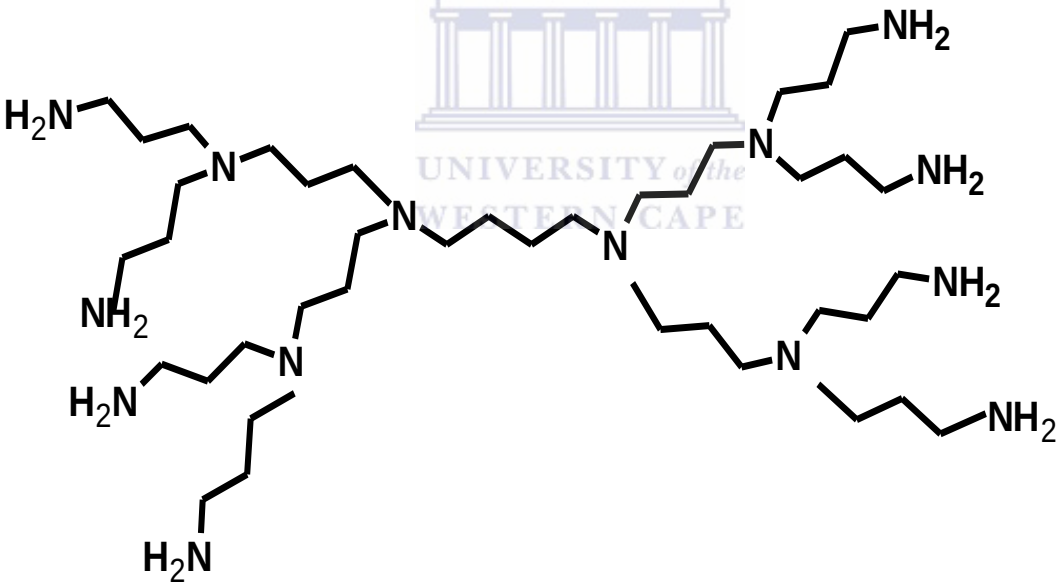

Figure 3: The structure of Poly(propylene imine) (PPI) dendrimer.

Poly(propylene imine) dendrimers are synthesized by the divergent method and are grown by reiterative sequence consisting of a double Michael addition of acrylonitrile to the

primary amino groups followed by hydrogenation under pressure in the presence of Raney cobalt **[22, 23. 24]**. Poly(propylene imine) (PPI) dendrimers are highly branched macromolecules terminated with amino groups with a number of interesting characteristics **[25, 26]**. They can be used as hydrogen donors because of their high density of amino groups. Dendrimers, with their easily accessible multiple terminal or end functional group, are ideal for the construction of star-shaped polymers **[25]**. PPI dendrimers are of interest due to their unusual physical properties **[27]**. An important physical feature of PPI dendrimers is that their viscosity in solution and in melt is lower than that of linear polymers, and that the viscosity decreases with increase in molecular weight **[28]**. Theoretical studies of the PPI dendrimers have given rise to predictions of attractive properties of the molecule depending on the pH and salt concentration of the aqueous environment **[25]**. At low pH and low salt concentration, the interior tertiary amine groups are protonated leading to a repulsion of charges. This repulsion results in what is considered as an "extended conformation" of the PPI dendrimer. At high pH and high salt concentration, the tertiary amine groups are no longer protonated, leading to a collapse of the dendrimer onto itself **[25]**. Dendrimers have an important property, which is their tendency to form cationic structures under physiological conditions (pH 7.4). Under such conditions the primary amines on the surface of the dendrimer protonate readily **[25]**.

The surface functionalities and core of the PPI dendrimers can be modified for a variety of applications, such as, molecular electronics, molecular recognition, catalysis, electroluminescent devices and sensors **[29]**. The σ bond- π bond conjugation of PPI dendrimers makes them ideal electron mediators, this property together with their high

compatibility with proteins, such as, enzymes, makes PPI dendrimers useful in the construction of biosensors **[29, 30]**.

Different generations of dendrimers can be synthesized. The number of functional groups on the dendrimer surface increase exponentially as a function of generation, generation 1 PPI dendrimer has four functional groups while generation 2 PPI dendrimer has eight **[25]**. Higher generations have interior void spaces that large enough to accommodate nanoscopic guests of various kinds. Generation 2 PPI dendrimer has more spaces to accommodate guests than generation 1 PPI dendrimer **[25]**.

2.5. Cytochrome P450 2E1

The Cytochrome P450 constitutes a super-family of heme-containing enzymes that catalyze the metabolism of a wide variety of endogenous and xenobiotic compounds **[31, 32-33]**. This is accomplished through the activation of molecular oxygen by the heme group, a process that involves the delivery of two electrons to the P450 system followed by cleavage of the dioxygen bond, yielding water and an activated iron-oxygen species which reacts with substrates through a variety of mechanisms **[34].** Cytochrome P450 enzymes are responsible for the hydroxylation of a number of compounds including steroids, fatty acids, drugs, food additives, fungi, bacteria, alkanes and polyaromatic and polychlorinated hydrocarbons **[32, 35]**.

In man most of the cytochrome P450 enzymes are found in the liver with a remarkable amount also found in the small intestine, around the microsomal part of the cytoplasm, in the endoplasmic reticulum as well as in the mitochondria **[36]**. Enzymes isolated from the

mitochondria are known as steroidogenic cytochrome enzymes since they are situated in single cell organisms and are phylogenetically older. Usually they consist of an iron-sulphur protein, NADPH and NADH-dependant reductase and cytochrome P450 enzyme **[32]**. Xenobiotic enzymes are located in the smooth endoplasmic reticulum of cells, while some studies indicate that they have evolved during the period of plant-animal differentiation. They are constituted by NADPH: P450 reductase (FAD-and FMN-containing flavoprotein) and cytochrome P450 enzyme. The strength of these enzymes lies in their ability to metabolize foreign biological substances **[37]**.

Cytochrome P450 2E1 (CYP2E1) is a member of the cytochrome P450 enzymes with diverse origins where they can be of bacterial, microsomal and mitochondrial origin **[38]**. CYP2E1 plays a role in the oxidative metabolism of a small range of substrates, solvents, and anaesthetics; these are a few of many important drug interactions mediated by CYP2E1 **[32]**. CYP2E1 has the smallest active site amongst all human cytochrome enzymes; this is consistent with the low molecular weights of many CYP2E1 substrates **[32]**. Among the available cytochrome P450 enzymes, CYP2E1 is notable for resulting in liver toxicity, due to the fact that CYP2E1 consists of over 50 % of the hepatic cytochrome P450 mRNA and 7 % of the hepatic cytochrome P450 protein **[35]**. CYP enzymes are associated with different types of reactions such as hydroxylation, epoxidation, dehalogenation, dehydrogenation and N-dealkylation which, together with the monooxygenation capabilities, has resulted in their application in biosensors and bioreactors **[32]**. In this study CYP2E1 employed for metabolism of pyrazinamide, an antituberculosis drug. Table1 indicates substrates, inducers and inhibitors of CYP2E1 while the structure of CYP 2E1 is illustrated in Figure 3.

Table 1: Substrates, inducers and inhibitors of CYP2E1

Substrates	Inhibitors	Inducers
Anaesthetics: ❖ Halothane ❖ Enflurane ❖ Isoflurane	**Strong:** Diethyldithiocarbamate	➢ Acetone ➢ Ethanol ➢ Isoniazid
Other: • Paracetamol • Dapsone • Theophylline • Ethanol • Ohlorzoxazone • Toluene • Isoniazid	**Unspecified:** ➢ Cimetidine ➢ Disulfiram	

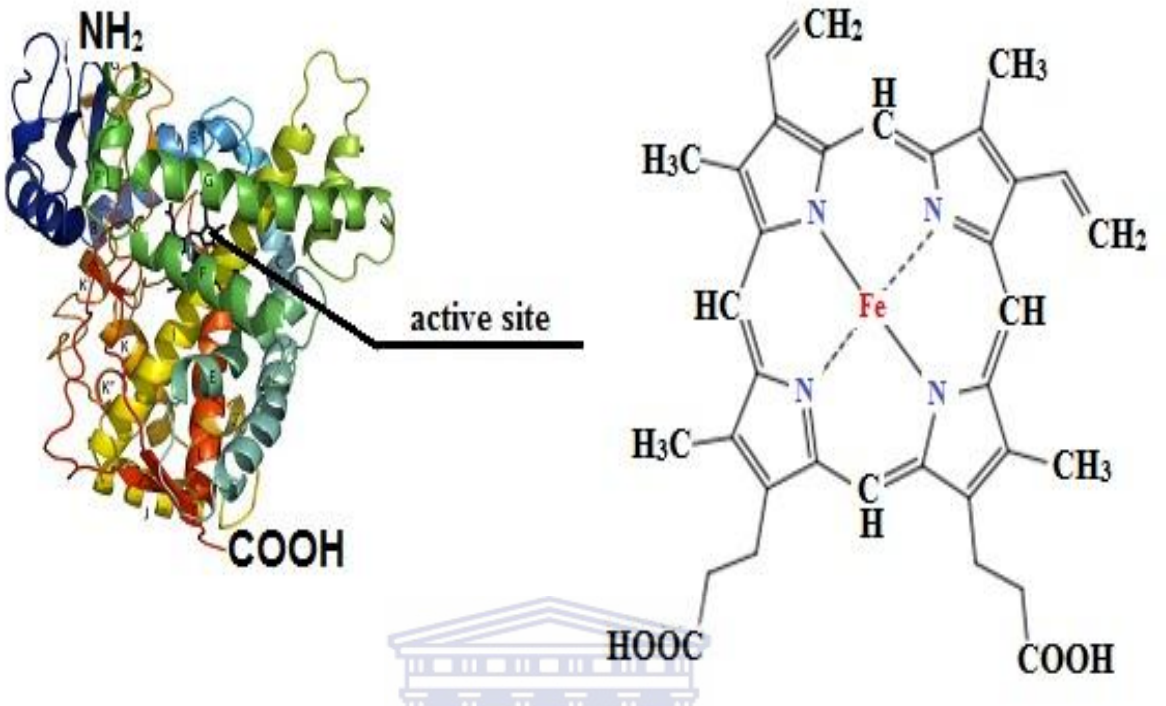

Figure 4: Distal face of CYP2E1 rainbow colored from N terminus (blue) to C terminus (red) also showing the active site of CYP2E1 **[32]**.

2.5.1. Kinetics of catalytic reaction of CYP enzymes:

Cytochrome P450 enzymes (**Figure 4**) consist of iron-protoporphyrin IX active sites with axial thiolate of cysteine residues as fifth ligands. Cytochrome P450 enzymes at rest are in the ferric form (Fe^{3+}), one electron reduction of the ferric form leads to a ferrous state (Fe^{2+}). In most cases, these enzymes are octahedral and because of unpaired electrons in their 3d orbitals, they are practically all paramagnetic **[33, 34-35]**. Due to the presence of protoporphyrin IX, heme enzymes exhibit characteristic visible absorption spectra however, their spectra differ according to the identities of the lower axial ligands donated by the protein and the oxidation state of the iron, while the identities of the upper axial

ligands are donated by the substrates. The source of electrons in this type of system is from flavoproteins, ferrodoxin like proteins, NADPH, the mediator or an electrode **[32]**.

The mechanism for substrate hydroxylation by cytochrome enzymes, involves the following steps although there are still several details that still remain unsolved.

- 1st Step: When the substrate binds to the hexa-coordinated low-spin ferric enzyme, water is excluded from the active site resulting in a change in the 5-coordinate low spin state. This causes a decrease in polarity which is accompanied by the lowering of the redox potential by 110 mV to 130 mV which makes the first electron transfer step thermodynamically favourable, from its redox partner NADH or NADPH

- 2nd step: The transfer of the first electron from one of the redox partners reduces the ferric iron to the ferrous enzyme and this process is called reduction.

- 3rd step: This form of the enzyme can now bind molecular oxygen resulting in a ferrous-dioxygen (Fe^{2+}- O_2) complex.

- 4th step: The O_2^{2-}reacts with two protons from the surrounding solvent, thereby breaking the O-O bond to release a water molecule and a highly active iron-oxoferryl intermediate.

- 5th step: One hydrogen atom is abstracted from the substrate by the intermediate to produce a one electron reduced ferryl species (Fe^{IV}- OH) and a substrate radical. On the other hand, the ferryl species reacts with the C – H bond of the substrate in a concerted reaction without the radical intermediate formation.

- 6th step: The final step of the process is the formation of the enzyme product complex and the release of the product. The low-spin state of the enzyme is then regenerated

The reaction mechanism of the CYP enzymes is illustrated in the following scheme:

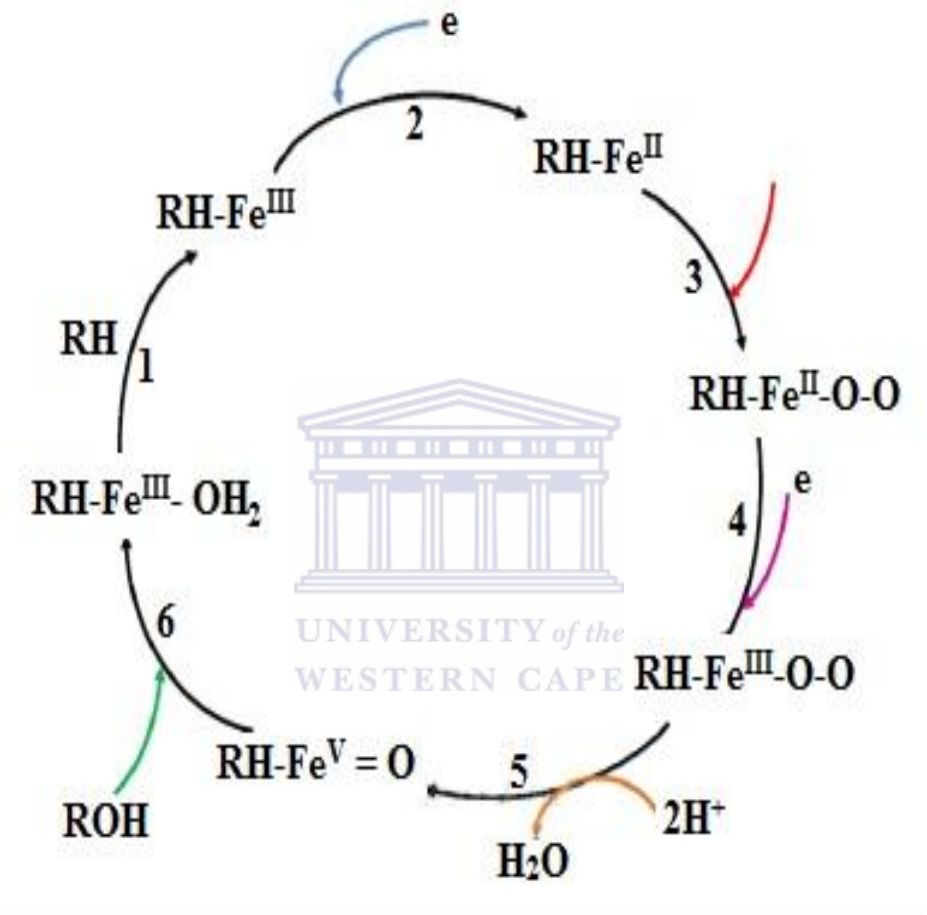

Scheme 3: The mechanism pathway of CYP enzymes **[32]**.

CHAPTER 3

EXPERIMENTAL METHODS

Summary

This chapter outlines the synthesis of second generation poly(propylene imine) dendrimer, nickel-poly(propylene imine) metallodendrimer and nickel-poly(propylene imine)-co-polypyrrole star copolymer using appropriate reagents and routes as discussed below. The method of biosensor fabrication by immobilization of the CYP2E1 enzyme onto the star co-polymer platform is also stated. Finally, the star copolymer and its respective individual components were characterized using electrochemical, spectroscopic (FTIR and XRD) and microscopic (TEM and SEM) techniques.

3.1. Reagents

Reagent grade pyrrole (98%), pyrrole-2-aldehyde (98%), dichloromethane (98%), methanol (›99.9%), lithium per chlorate (99.9%), sodium phosphate dibasic dihydrate ($HNa_2O_4P.2H_2O$ ~ ≥99.5%), sodium phosphate monobasic dihydrate ($H_2NaO_4P.2H_2O$ ~ ≥99%), nickel chloride hexahydrate ($NiCl_2.6H_2O$ ~ 99.99%) and Generation 2 poly(propylene imine) dendrimer were purchased from Sigma Aldrich. Ethanol (96.4%) was purchased from Kimix. Grade I 25% glutaraldehyde was purchased from sigma Aldrich. Bovin serum albumin (BSA) was purchased from Fluka. Alumina micro polishing pads were obtained from Buehler. Stock enzyme solutions of 2μM CYP2E1 were prepared from CYP2E1 solution from sigma Aldrich (C5740). Stock solution of pyrazinamide was prepared from a 30 mg pyrazinamide powder from Sigma Aldrich. De-ionized water, used throughout the experiments, was prepared with a Milli-Q water

purification system. Analytical grade argon gas, obtained from Afrox South Africa, was used for degassing the cell solutions.

3.2. Instrumentation

All electrochemical measurements were done using BASi epsilon from Bio Analytical Systems (BAS), Lafayette, USA. All cyclic voltammograms were recorded with a computer interfaced to BASi epsilon using a 10 mL electrochemical cell with a three-electrode set up. The electrodes used in the study were (1) a platinum working electrode (A = 0.0201 cm^2) from BAS, (2) platinum wire counter electrode from Sigma Aldrich and (3) a Ag/AgCl (kept in 3 M NaCl) reference electrode from BAS. Alumina micro polishing pads were obtained from Buehler, LL, USA and were used for polishing the platinum electrode before modification. HRTEM images were taken using Tecnai G2 F20X-Twin MAT 200kV Field Emission Transmission Microscopy from FEI (Eindhoven, Netherlands).All FTIR spectra were recorded on Spectrum 100 FTIR spectrometer (PerkinElmer, USA) in a region of 400 to 4000 cm^{-1}. All samples were dried using Buchi rotarvapor and buchi waterbath from Labotech.

3.2.1. Electrochemical techniques

Electrochemical techniques are used to interrogate the redox properties of the biosensors and their prospective platform components at the electrode surface which occur when a potential is applied. From the redox behaviour of different materials under different conditions, various parameters such as rate constant, diffusion coefficient, formal potential, film thickness, sensitivity, detection limits, surface concentration, solution

resistance, charge transfer resistance and process reversibility can be determined. However, the main limitation of voltammetric techniques is that the species under investigation must be either reducible or oxidizable in the range where both the electrode and the electrolyte are electrochemically inert.

3.2.1.1. Cyclic voltammetry

Amongst the electrochemical techniques, cyclic voltammetry (CV) has become an important and widely used versatile electroanalytical technique in many areas of chemistry **[39, 40]**. CV is used to investigate kinetics for understanding reaction intermediates, and for obtaining stability of reaction products and mechanisms of various reactions at electrode surfaces. This technique is also used in the measurement of kinetic rates and constants and determination of adsorption processes on surfaces, electron transfer and reaction mechanisms **[25, 32]**. This technique is based on altering the applied potential (E) at a working electrode in both the forward and reverse directions while applying different scan rates and monitoring the current (I). In many cases, the applied potential (E) is changed or the current is monitored over a period of time (t). Thus, all voltammetric techniques can be described as some function of E, I, and t. They are considered active techniques (as opposed to passive techniques such as potentiometry) due to the fact that the applied potential forces a change in the concentration of an electroactive species at the electrode surface by electrochemically reducing or oxidizing it **[41, 42]**. CV has a major drawback, which is the reduced sensitivity at very low levels of analyte concentration, brought about by currents caused by double-layer effects and other sources **[41]**. The most important parameters in a cyclic voltammogram are the peak

potentials (E_{pa}, E_{pc}) and peak currents (I_{pa}, I_{pc}) of the anodic and cathodic peaks, respectively. If the electron transfer process is fast compared with other processes (such as diffusion), the reaction is said to be electrochemically reversible, and the peak separation is given by:

$$\Delta E_p = \left|E_{p,c} - E_{p,a}\right| = {}^{2.303\ RT}/_{nF} \qquad \text{Equation (1)}$$

where ΔE_p = peak separation, E_{pc} = cathodic peak potential, E_{pa} = anodic peak potential, R = Gas Constant (8.314 J/M/K), T = absolute temperature (298.15 K), n = number of electrons (1), F = Faraday constant (96485 C/mol)

therefore, for a reversible redox reaction at 25 °C with n electrons ΔE_p should be 0.0592 /nV **[22]**.

The formal reduction potential (E^o) for a reversible couple is given by:

$$E^\circ = \frac{E_{p,c}+E_{p,a}}{2} \qquad \text{Equation (2)}$$

Cyclic voltammograms, from this study, showed increased peak currents and potential shifts for the Ni-PPI-co-PPy than pure Ppy. PPI-2Py increased the effect of redox reactions on PPY when it was used to form a PPI-co-Py star copolymer; this was observed by increased peak currents after the electrochemical formation of the star copolymer **[25]**. This behaviour is attributed to the intrusion of the Ni-PPI metallodendrimer into the polymer backbone of PPy which alters its electronic properties by increasing the single

bond and double bond conjugation and thus increase the number of charge carriers, thereby leading to enhanced electrochemically activity of the copolymer.

3.2.2. Spectroscopic techniques

Spectroscopic techniques employ light to interact with matter and thus probe certain features of a sample to learn about its consistency or structure. Light is electromagnetic radiation, a phenomenon exhibiting different energies, and dependent on that energy, different molecular features can be probed. Spectroscopic techniques are the most highly sensitive and are non-destructive to samples, require small sample volumes and do not require complex sample preparations of biological samples. These features make them highly applicable in the characterization of small sample volumes.

3.2.2.1. Fourier Transform Infra-Red spectroscopy (FTIR)

"Fourier spectroscopy" is a general term that is used to describe the analysis of any varying signal into its constituent frequency components. Using the mathematical methods that are named after J.B.J. Fourier, that are extremely powerful in spectroscopy, Fourier transforms can be applied to a variety of spectroscopies including infrared spectroscopy known as Fourier transform infrared (FT-IR), nuclear magnetic resonance (NMR), and electron spin resonance (ESR) spectroscopy **[25]**.

FTIR is most useful for identifying the identifying types of chemical bonds (functional groups). It can be applied to the analysis of solids, liquids, and gasses. In infrared spectroscopy, IR radiation is passed through a sample, some of the infrared radiation is absorbed by the sample and some of it is passed through (transmitted). The wavelength of

light absorbed is characteristic of the chemical bond. The resulting spectrum represents the molecular absorption and transmission **[3]**. The spectrum works like a molecular fingerprint of the sample and a fingerprint is unique for each molecule, no two unique molecular structures produce the same infrared spectrum. This makes infrared spectroscopy useful for several types of analysis. FTIR was used to characterise PPI dendrimer, PPI-2Py dendrimer and PP-co-PPY star copolymer, the spectra of the moieties were recorded in the region 400 to 4000 cm^{-1}, without mixing with KBr. The spectra obtained were used to identify the various functional groups in the star copolymer as well as those in the backbone chain of the dendrimers **[25]**.

3.2.3. Microscopic techniques

3.2.3.1 High resolution scanning electron microscopy (HRSEM)

The HRSEM is one of the most flexible instruments available used for the examination or analysis of the morphology of nanomolecules and chemical composition characterization. HRSEM uses electrons rather than light to form an image of objects such as fractured metal components, foreign particles and residues, polymers and biological samples, among others **[3]**. It uses a focused beam of high energy electrons to generate a variety of signals at the surface of solid specimens **[41]**. In the HRSEM the electron beam traces over the object and interacts with the surface of the object, dislodging secondary electrons from the surface of the specimen in unique patterns. A secondary electron detector attracts those scattered electrons and, depending on the number of electrons that reach the detector, registers different levels of brightness on a monitor **[42]**. Additional sensors

detect backscattered electrons (electrons that reflect off the specimen's surface) and X-rays (emitted from beneath the specimen's surface). Dot by dot, row by row, an image of the original object is scanned onto a monitor for viewing **[41]**. The advantages associated with HRSEM include, among others, its ability to perform analysis of selected point locations on the sample and that it is non-destructive of the sample **[3]**. Areas ranging from approximately 1 cm to 5 microns can also be imaged in a scanning mode using conventional SEM techniques (magnification ranging from 20×to approximately 30,000×, and a spatial resolution of 50 to 100 nm). In the study it was used for the determination of the surface morphologies of G2 PPI-PPy and nickel-PPI-2Py metallodendrimer. SEM was used to study the morphology of PPI-co-PPY [81]. SEM was used for the characterization of poly(propylene imine)-based rhodium (I) metallodendrimers **[26]**.

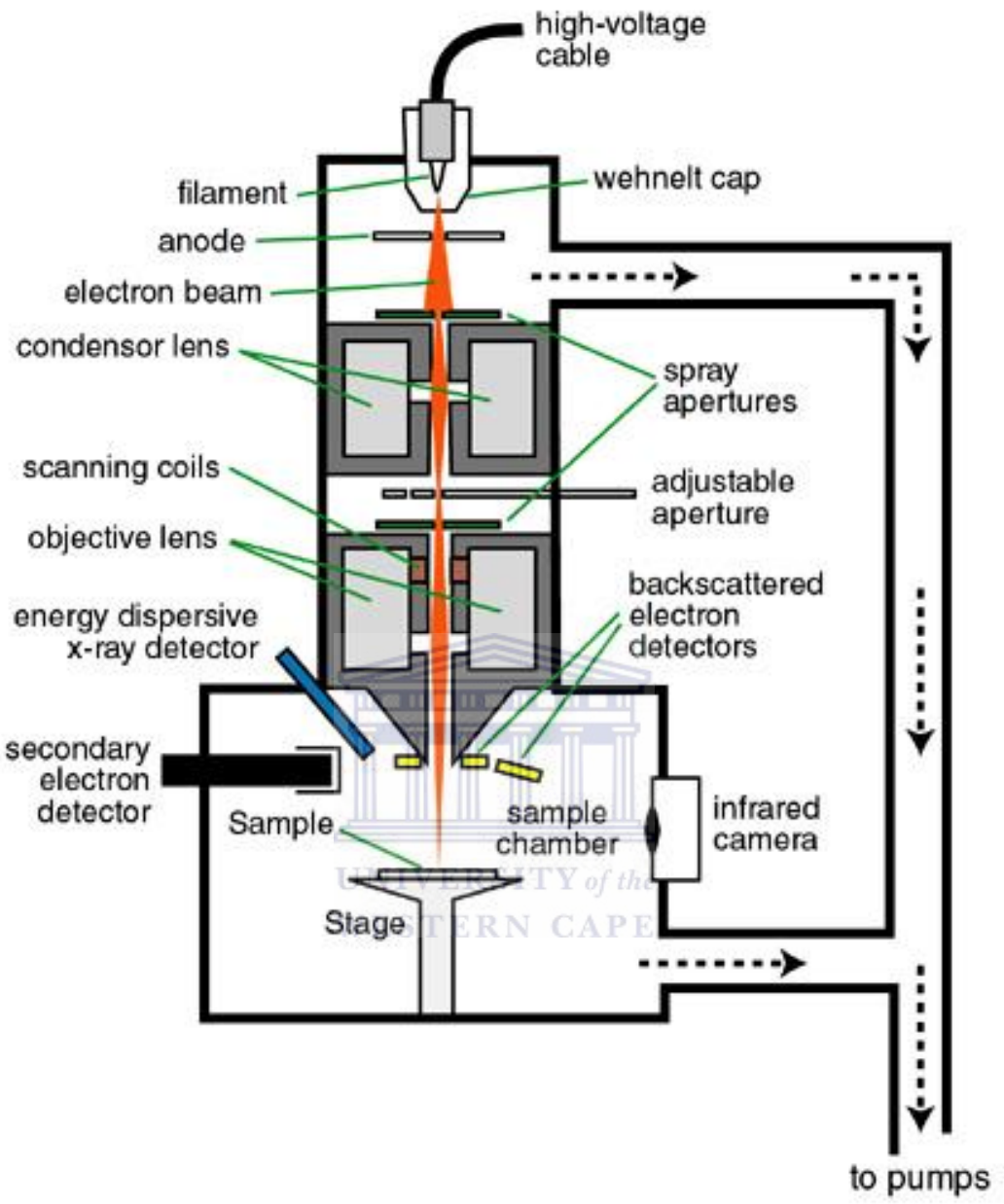

Scheme 4: Parts of the SEM instrument **[43]**.

3.2.3.2. High resolution transmission electron microscopy (HRTEM)

In the TEM, only thin samples (which allow a fraction of the incident electron beam to go through them) can be studied. When an accelerated beam of electrons impinges upon a sample, a rich variety of interactions takes place **[3]**. The versatility of electron

microscopy and X-ray microanalysis is derived in large measure from this variety of interactions that the beam electrons undergo in the specimen.

HRTEM is a microscopic technique operational when a beam of electrons is transmitted through an ultra-thin sample material, interacting with the sample as it passes through. The electrons behave as a light source with much lower wavelengths, making it possible to obtain resolutions a thousand times better than using light microscopes **[42]**. Depending on the density of the material present, some of the electrons are scattered and disappear from the beam, while at the bottom of the microscope, the unscattered electrons hit a fluorescent screen which gives rise to a "shadow image" of the sample in question with its different parts displayed in varied darkness according to their respective densities**[41]**. The interaction of the electrons with the sample creates an image which is magnified and focused onto an imaging device, such as a layer of photographic film, a fluorescent screen or to be detected by a sensor such as a CCD camera **[25]**. This instrument enables users to examine fine details, even as small as a single column of atoms, which is tens of thousands times smaller than the smallest resolvable object in a light microscope. This technique uses phase contrast resulting from an interference of several beams and determines whether the particle that makes the specimen are dispersed or agglomerated **[32]**. The technique is limited in high magnification imaging which requires high electron dose where by the specimen needs to be relatively insensitive. In this study HRTEM was used to confirm the size, shape and distribution of nickel-PPI-2Py metallodendrimer.

3.2.3.3. Energy Dispersive x-ray Spectroscopy (EDS)

X-rays are electromagnetic radiations with wavelengths between 10^{-8} m and 10^{-12} m. They are part of the electromagnetic spectrum that includes wavelengths of electromagnetic radiation called visible light **[44, 45-46]**.

The energy-dispersive X-ray spectroscopy (EDS, EDX, or XEDS), sometimes called energy dispersive X-ray analysis (EDXA) or energy dispersive X-ray microanalysis (EDXMA), is an analytical technique that can be coupled with HRSEM, HRTEM and Scanning Transmission Electron Microscopy (STEM) **[44, 47]**. When EDS is coupled with these imaging techniques, it can be used as an elemental analysis tool that is able to analyse samples as small as nanometers in diameter **[47]**. In EDS the impact of electron beam, from any of the above mentioned imaging techniques, on the sample produces X-rays that are characteristic of the elements that form the sample. Its characterization capabilities are due in large part to the fundamental principle that each element has a unique atomic structure, allowing unique set of peaks on its X-ray emission spectrum . To stimulate the emission of characteristic X-rays from a specimen, a high-energy beam of charged particles such as electrons, protons or X-rays, is focused into the sample being studied **[44, 47]**. At rest, an atom within the sample contains ground state electrons in discrete energy levels or electron shells bound to the nucleus. The incident beam may excite an electron in an inner shell, ejecting it from the shell while creating an electron hole where the electron was **[47]**. An electron from an outer, higher energy shell then fills the hole, and the difference in energy between the higher energy shell and the lower energy shell may be released in the form of an X-ray. The number and energy of the X-

rays emitted from a specimen can be measured by an energy-dispersive spectrometer **[44]**. As the energy of the X-rays is characteristic of the difference in energy between the two shells, and of the atomic structure of the element from which they were emitted, this allows the elemental composition of the specimen to be measured **[47]**. The EDS was used in this study to study the elemental properties of the Ni-PPI-2Py metallodendrimer.

3.3. Methodology

3.3.1. Synthesis of 2-pyrrole-functionalized second generation poly(propylene imine) dendrimer to G2 (PPI-2Py).

The synthesis of PPI-2Py was carried out by, initially, a condensation reaction of PPI with 2-pyrrole aldehyde. A reaction mixture containing PPI generation 2 (0.8886 g, 1.149 mMol) and 2-pyrrole aldehyde (0.87144g, 9.149 mMol) in 50 mL dry methanol (50 mL) was magnetically stirred under a positive pressure of nitrogen gas for 2 days in a 100 mL 3-necked round bottom flask. The methanol was removed by rotary evaporation, the residual oil was dissolved in 50 ml dichloromethane (DCM), and the organic phase was then washed with water (6 × 50 mL) to remove unreacted monomer. The DCM was removed by rotary evaporation and yielded the desired product, PPI-2Py**,** as orange oil.

3.3.2. Synthesis of generation 2 Ni metallodendrimer (Ni-PPI-2Py)

PPI-2Py (0.0880 g) was dissolved in ethanol (10 mL) in around bottom flask, under nitrogen. Nickel (II) chloride hexahydrate (0.064 g) was added to the solution and the reaction mixture was refluxed under nitrogen for 24 h. The solvent was evaporated via

rotary evaporation, yielding a green residue. The residue was dissolved in dichloromethane (DCM) (15 mL) and the solution was filtered by gravity filtration. The solvent was removed from the filtrate, producing a green solid which was washed with hexane (3 x 5 mL). The product was dried under vacuum, yielding a brown solid. The solid was dissolved in 1:2 methanol/ DCM mixture.

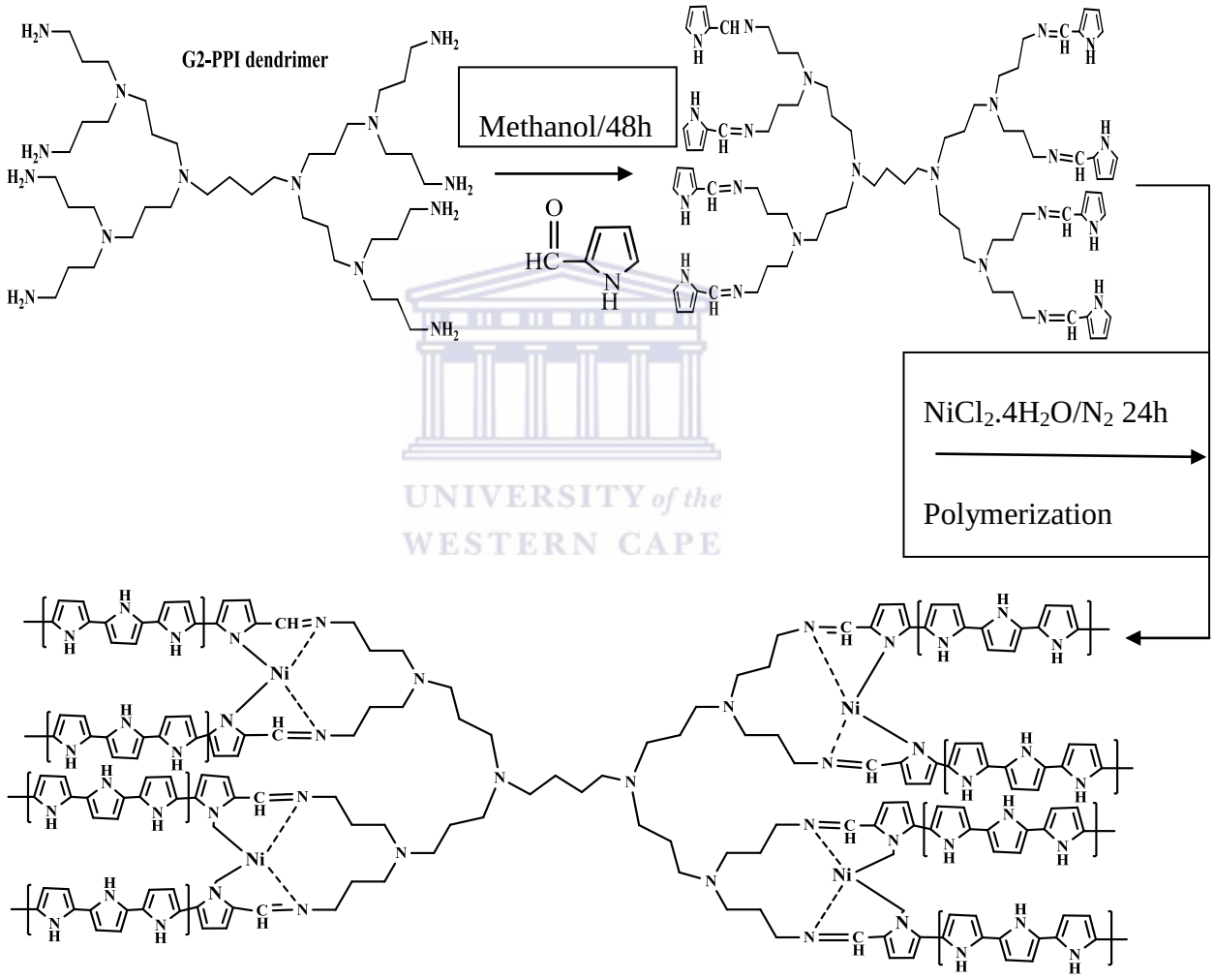

Scheme 4: The chemical synthesis of Ni-PPI-Ppy.

3.3.3. Pre-treatment of working electrode

A platinum working electrode was polished with 1 μm, 0.5 μm and 0.03 μm alumina slurries in glassy polishing pads, minimum for 5 min on each pad. After polishing, the electrode was ultra-sonicated for about 15 min with distilled water and absolute ethanol, respectively, to remove any possible absorbed alumina crystals on the electrode surface, followed by rinsing carefully with distilled water. The above procedure resulted into a clean platinum working electrode.

3.3.4. Preparation of Ni-PPI-PPy/Pt electrode

3 μL Ni-PPI-2py was drop-coated onto platinum working electrode and dried at room temperature for 4 h. Onto the Ni-PPI-2Py/Pt electrode, polypyrrole was prepared by electropolymerization of the pyrrole monomer in 0.1 M $LiClO_4$ supporting electrolyte. Polymerization was done at a potential of -800mV to +800 mV (vs Ag/AgCl) at a scan rate of 50mV/s for 30 cycles.

3.3.5. Fabrication of CYP2E1 biosensor: Ni-PPI-PPy/CYP2E1/BSA/Glu/Pt

CYP2E1 was immobilized on the Ni-PPI-PPy/Pt by drop-coating. 3 μL of a 1M CYP2E1 enzyme solution, containing 2.0 mg BSA was carefully drop-coated onto the Ni-PPI-PPy modified Pt electrode. 2 μL of 2.5% glutaraldehyde solution was drop coated onto modified electrode. The enzyme-modified electrode was then covered with a tight fitting lid for the first 10 minutes to form a uniform layer, after which, the lid was removed and the enzyme layer was slightly dried for 40 min but still retaining wet camera after which

the prepared biosensor was immediately placed at 4 ^{o}C for at least 60 min. The CYP2E1-based biosensor was denoted as Ni-PPI-PPy/CYP2E1/BSA/Glu/Pt.

For comparison, a biosensor based on CYP2E1 only (fabricated onto the bare platinum electrode, denoted as **CYP2E1/Pt**) was fabricated as follows:

3 μL of a 1 M CYP2E1 enzyme solution, containing 2.0 mg BSA was carefully drop-coated onto the clean Pt electrode. 2 μL of 2.5% glutaraldehyde solution was drop-coated onto the resulting electrode. The enzyme modified electrode was covered in a tight fitting lid for first 10 minutes to allow the formation of a uniform layer. The lid was removed and the enzyme was allowed to dry for 4 h at 4 ^{o}C. The resulting electrode was rinsed with Phosphate buffer (PBS) to remove any physically adsorbed enzyme. The CYP2E1-based biosensor was denoted CYP2E1/Pt and was kept at 4 ^{o}C in 0.1 M PBS when not in use.

CHAPTER 4

RESULTS AND DISCUSSION

Summary

This chapter outlines and discusses the results obtained for the study based on developing the Ni-PPI-PPy/CYP2E1/BSA/Glu/Pt nanobiosensor for detection of pyrazinamide. This chapter deals specifically with the characterization of the structural, elemental and morphological properties of the biosensor platform using techniques such as FTIR, SEM, TEM, and EDS. The electrochemical studies of the nanobiosensor platform and the detection of PZA using CV are also included.

4.1. Structural and morphological characterization of the Platform

In the following section we will discuss the characterization use of the following techniques which, provides information regarding the elementary analysis, such as EDS, and morphological (Scanning electron microscopy and transmission electron microscopy) and structural (Furrier transformer infrared spectroscopy)

4.1.1. FTIR

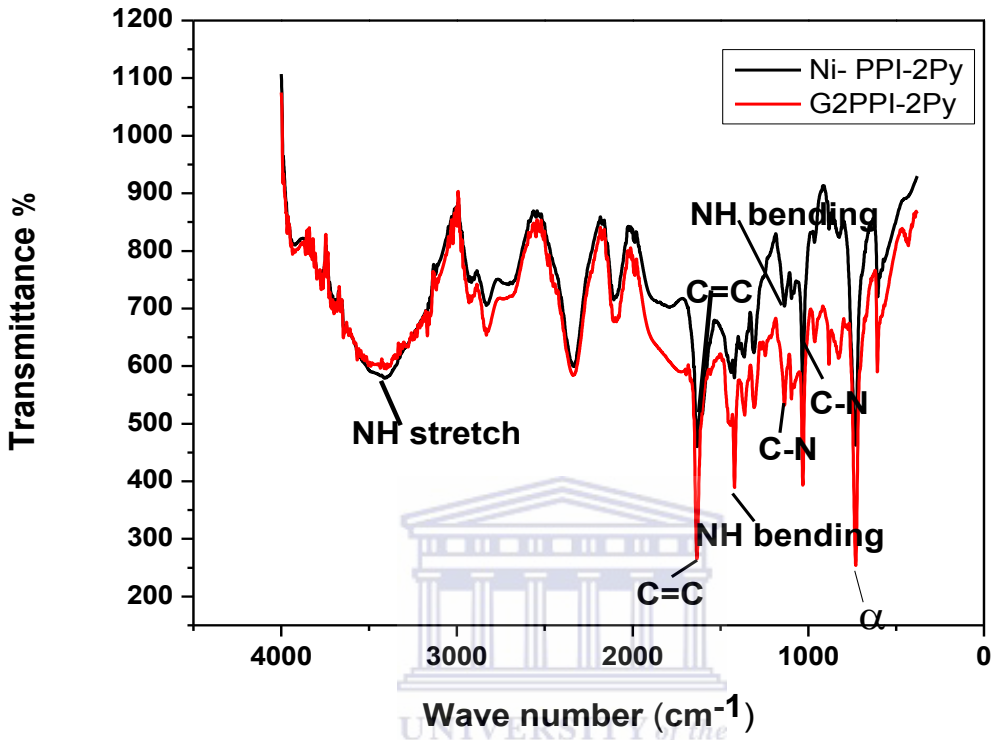

Figure 5: FTIR of Ni-poly(propylene imine) dendrimer (black) and G2 functionalized poly(propylene imine) dendrimer (red).

The FTIR spectra **(Figure 5)** of both Ni-PPI-2Py metallodendrimer and PPI-2Py show an out-of-plane bending of the C–H bond located at the α position in the pyrrole ring (729 cm^{-1}), and N=C band at 1634 cm^{-1} is assigned to the stretching vibration present in the dendrimer moiety **[25]**. The appearance of these two characteristic peaks confirms the functionalization of the amine groups of PPI by 2-Py.

The FTIR spectra of both the G2 PPI-2py and the Ni PPI-2Py show the characteristic (NH), ν(C=C), ν(C-N) aliphatic bond bands at, 3413 cm^{-1},1642 cm^{-1},1306 cm^{-1} of the

pyrrole ring respectively. The FTIR spectrum of the metallodendrimer shows no disappearance in any of the peaks of the dendrimer due to the fact that none of the dendrimer bonds were broken in the formation of the metallodendrimer. The vibrations associated with large metals bound to light ligand atoms (e.g.,metal-nitrogen, M-N) usually appear from 500 cm^{-1} to lower energies, the Ni-N bond normally appears within the broad range of 300 - 500 cm^{-1} **[48, 49]**. The dative bond Ni-N in the Ni-PPI-2Py metallodendrimer is a result of sharing of lone pairs of electron from the nitrogen atoms. Therefore in most cases this type of bond is referred to as an artificial bond **[49, 50]**. Dative bonds can sometimes be semi-polar and FTIR shows polar bonds **[51]**. This could be the reason why the Ni-N bond is not present in the metallodendrimer spectrum.

Frequency, cm^{-1}	**Bond Type**
3400-3250	**N-H**
1680-1640	**-C=C**
1335-1250	**C-N Stretch aromatic**
1600–1585	**C-C Stretch**
1250-1220	**C-N Stretch aliphatic**
2800-3000	**CH Stretch**
1640-1690	**C=N**

Table 2: Types of bonds present in both the dendrimer and metallodendrimer and the frequencies that they appear on.

4.1.2. Energy Dispersive X- Spectroscopy (EDS)

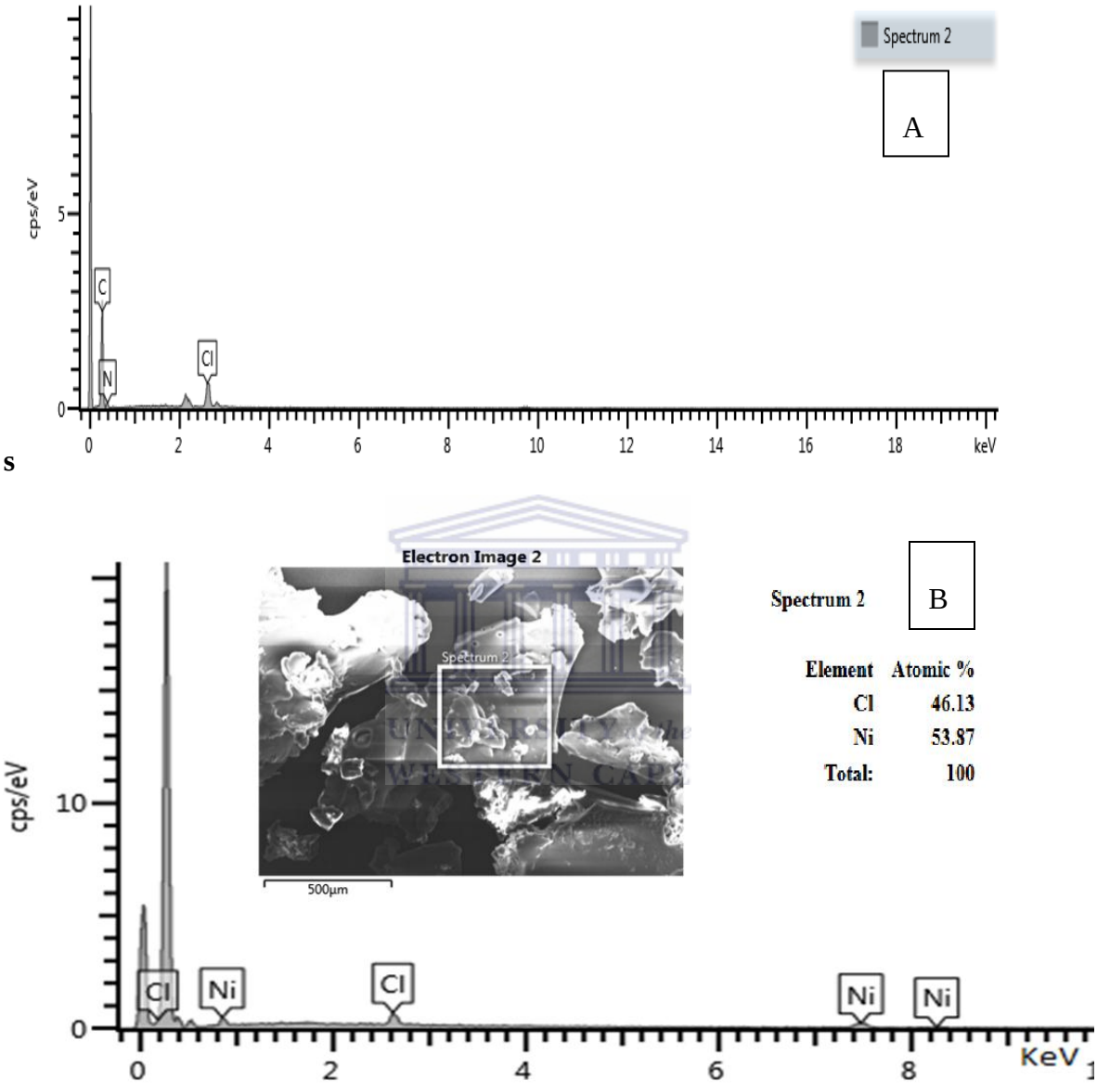

Figure 6: The Energy Dispersive X-ray spectrum of the (A) Ni-PPI-2py and (B) G2PPI-2Py.

The EDS was used to study the elemental composition of the Ni-PPI-2Py metallodendrimer and G2PPI-2Py dendrimer (**Figure 6A, B** respectively). The EDS spectrum (**Figure 5 A**) revealed that the most abundant elements in the metallodendrimer are nickel (Ni) and Cl respectively. The EDS also showed the presence of minute amounts of copper (Cu) and oxygen (O). The presence of both the Cl and O is due to the metal precursor $NiCl_2 \cdot 6H_2O$ used to introduce the metal into the dendrimer framework during synthesis. The copper is a result of the copper grid used to hold the sample during the analysis. The EDS spectrum of G2PPI-2Py (Figure 5 B) indicates that the material showed the presence of nitrogen and carbon atoms, with chlorine being the impurity that was present in the compound. Carbon and the nitrogen were expected as the structure of G2PPI-2Py contains nitrogen and carbon atoms only.

4.1.3. High resolution scanning electron microscopy (HR-SEM)

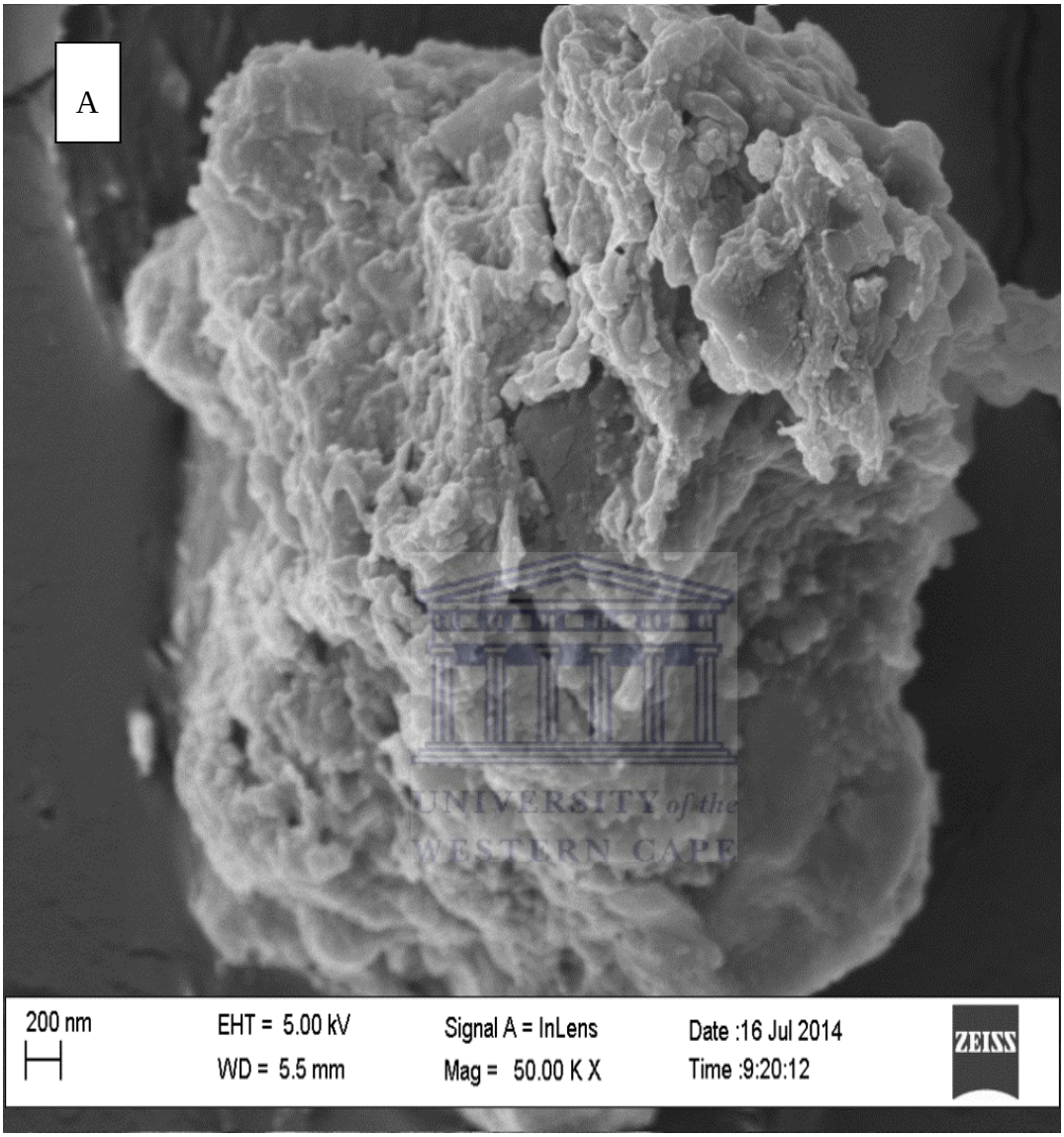

Figure 7(A): The HR-SEM image of the PPI-2Py.

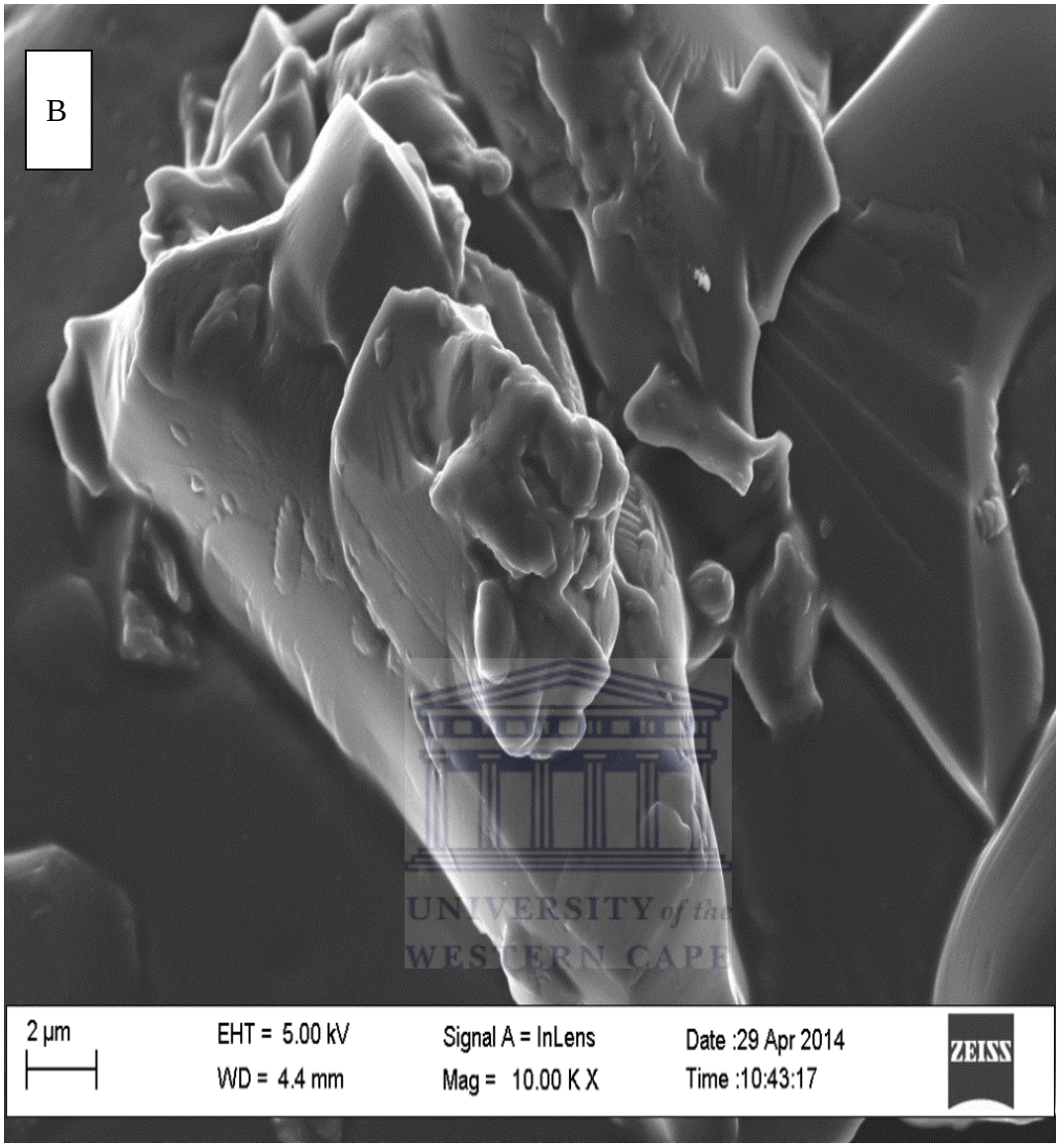

Figure 7(B): The HR-SEM image of the Ni-PPI-2Py.

The PPI-2Py had a sticky paste-like texture. The HR-SEM images of PPi-2Py and Ni-PPI-2Py (**Figure 7 A** and **B** respectively) show that the PPI-2Py and its morphology resembled that of densely clustered florets. The synthesis of the metallodendrimer required that the crystals be dissolved after collection. The morphology of the Ni-PPI-2Py shows that, after the incorporation of the metal into the dendrimer framework, crystals were formed. The

formation of crystals suggests that the Ni-PPI-2Py metallodendrimer was successfully synthesized.

4.1.4. High resolution transmission electron microscopy (HR-TEM)

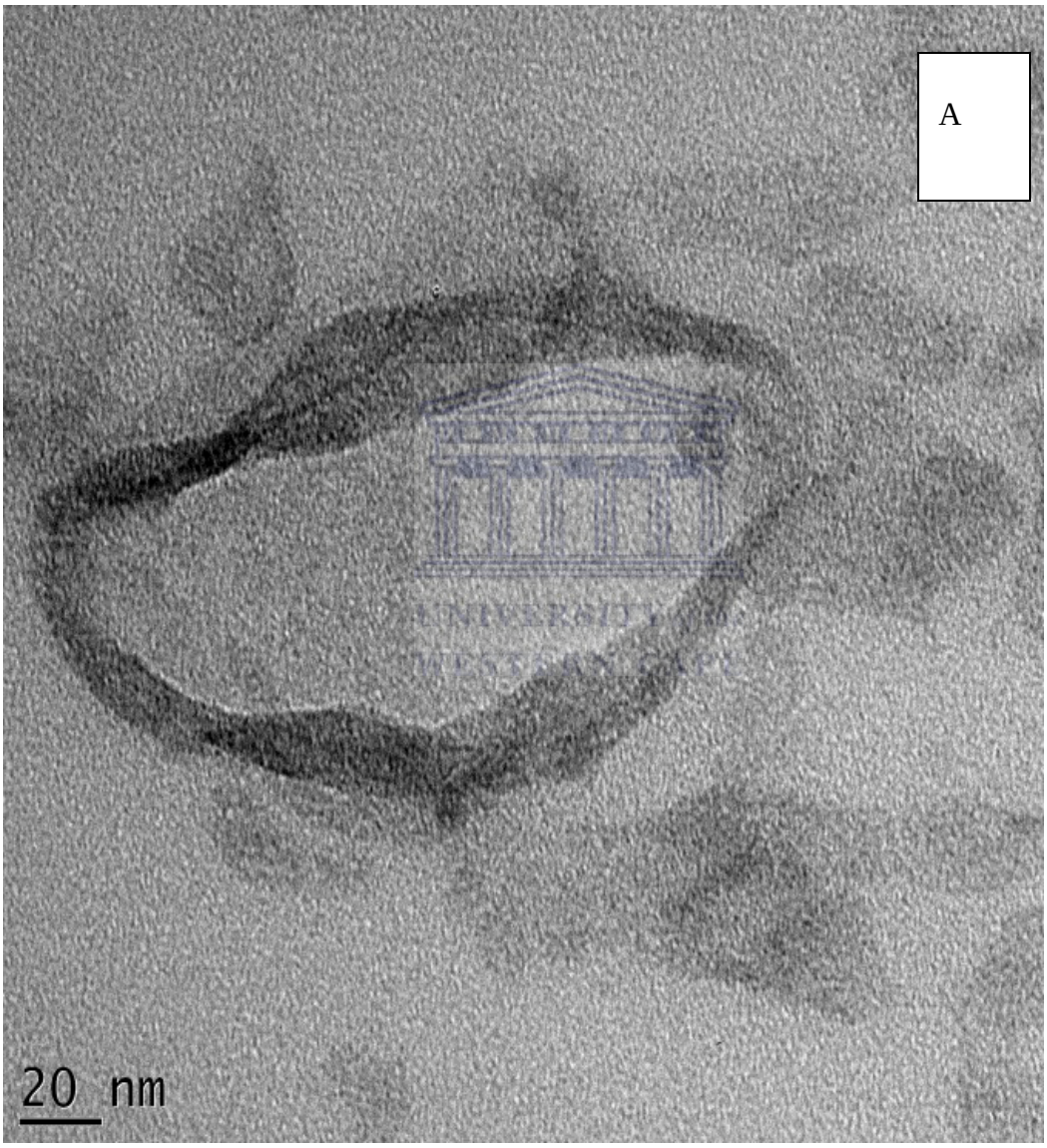

Figure 8(A): The HR-TEM micrograph of G2PPI-2Py.

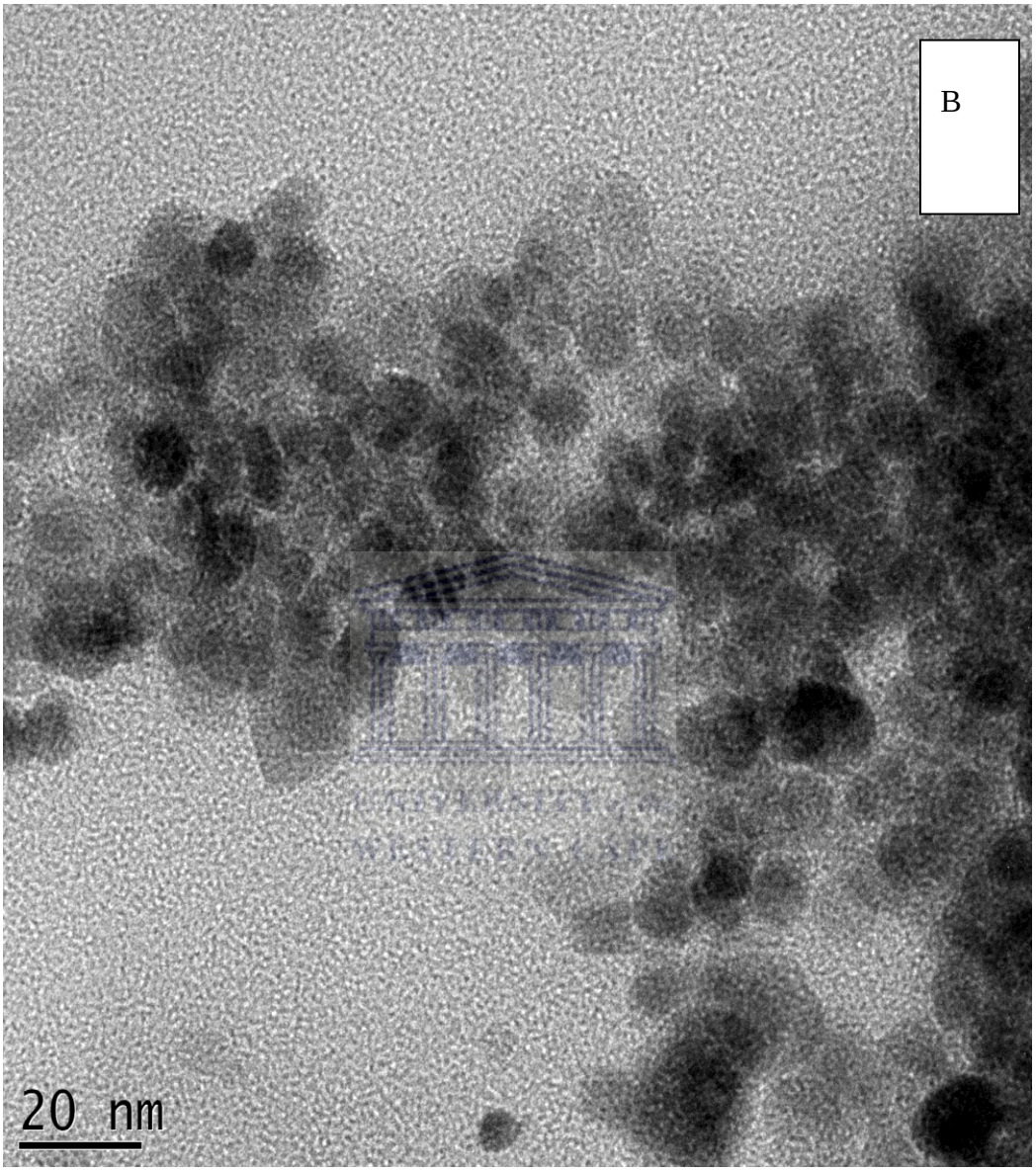

Figure 8(B): The HR-TEM micrograph of Ni-PPI-2Py.

HRTEM determines the shape and size of nanoparticles. In this study it was used to determine the size and shape of nickel nanoparticles present in the Ni-PPI-2Py complex. Figures 8A and B represent the internal structures of the G2PPI-2Py and the Ni-PPI-2Py

complexes. The structure of G2PPI-2Py shows the spherical shape of the dendrimer which is the typical shape of dendrimers. Figure 7B showed convincing results of shape, size and structure of the Ni-PPI-2Py metallodendrimer, observed with the 20 nm scale view. The micrograph showed that the crystals were poly-dispersed and their sizes were estimated to range between 10 and 16 nm, average being 12 nm. The shape of the metallodendrimer nanoparticles was mostly spherical and they are distributed as clusters.

4.2. Electrochemical studies of the platform using cyclic voltammetry (CV)

This section provides the discussion on the electrochemical studies of the platform. This includes the polymerization of the Ni-PPI-2py, the electrochemical studies of the polypyrrole, the electrochemical studies of the Ni-PPI-2Py and the detection of the pyrazinamide by the nanobiosensor.

4.2.1. Electropolymerization of polypyrrole

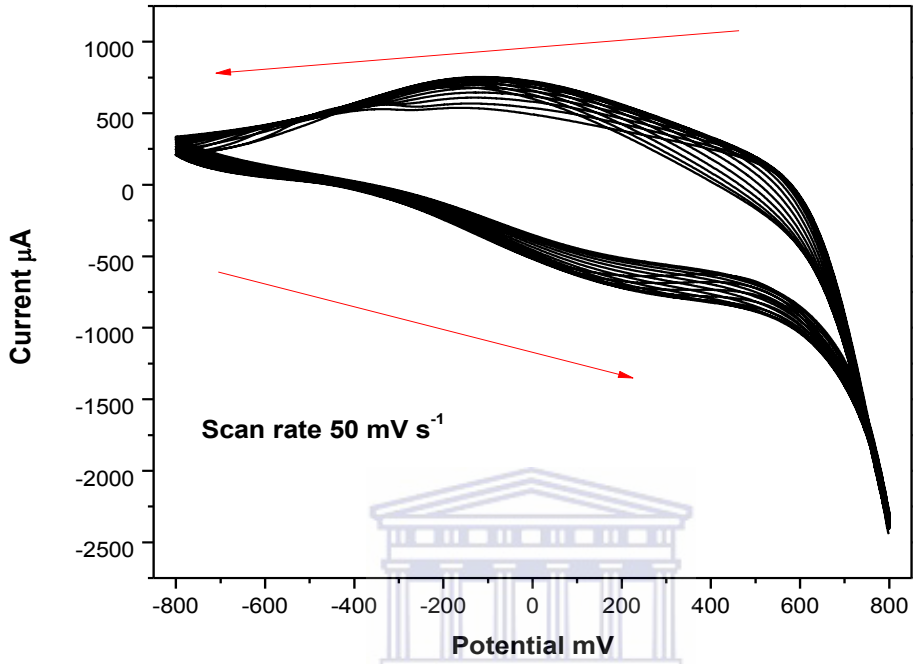

Figure 9: Electropolymerization of polypyrrole on the surface of Ni-PPI-2Py/Pt electrode, 20 cycles at 50 mV/s from -800 to 800 mV (vs. Ag/AgCl).

Figure 9 shows cyclic voltammograms for the electrochemical polymerization of pyrrole from +800 mV to -800 mV (vs Ag/AgCl) on Ni-PPI-2Py modified Pt electrode at a scan rate of 50 for 30 cycles in lithium perchlorate. At the initial oxidation step, the radical cation of the monomer is formed and reacts with other monomers present in solution to form oligomeric products and then the polymer. The current was observed to increase with increasing number of cycles, implying deposition of an electroactive material on the surface of the electrode. Growth of PPy is believed to take place from the α position of the

metallodendrimer, forming the Ni-PPI-co-PPY **[25]**. After the formation of black colored polymer film on the surface of the Ni-PPI-2Py, the electrode was taken out.

4.2.2. Electrochemistry of polypyrrole

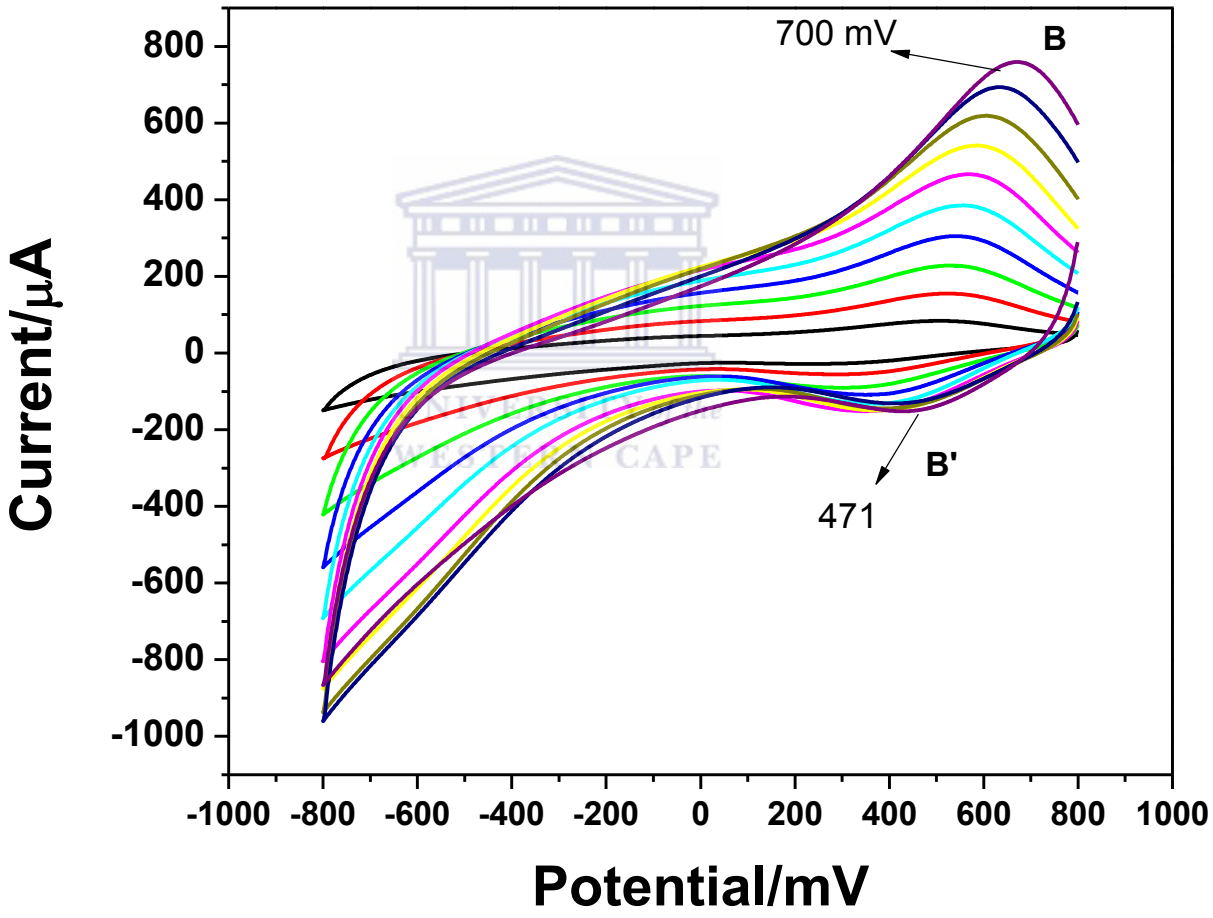

Figure 10: The Cyclic Voltammogram of polypyrrole in 0.1 M phosphate buffer. Taken from scan rates of 10-100 mV/s with 10 mV/s increments from -800 mV to +800 mV.

Figure 10 represents the cyclic voltammogram of polypyrrole in 0.1 M phosphate buffer pH 7.4 on the potential window of -800 mV to +800 mV. In the voltammogram there are two observable peaks, namely B and B'. The anodic peak B, at +700 mV is due to the oxidation of the pyrrole while the cathodic peak B' at +471 mV is due to the deposited pyrrole onto the electrode surface. There is a shift of the anodic potential towards more positive potential with an increase in scan rate from +550 to +700 mV giving evidence of a more readily oxidised species. There is also an observable linear increase in the anodic peak current with an increase in scan rate, shown in figure 9, which indicates the occurrence of the electrochemistry of surface confined species. No shift in the cathodic peak current is observed; this indicates the presence a surface bound species.

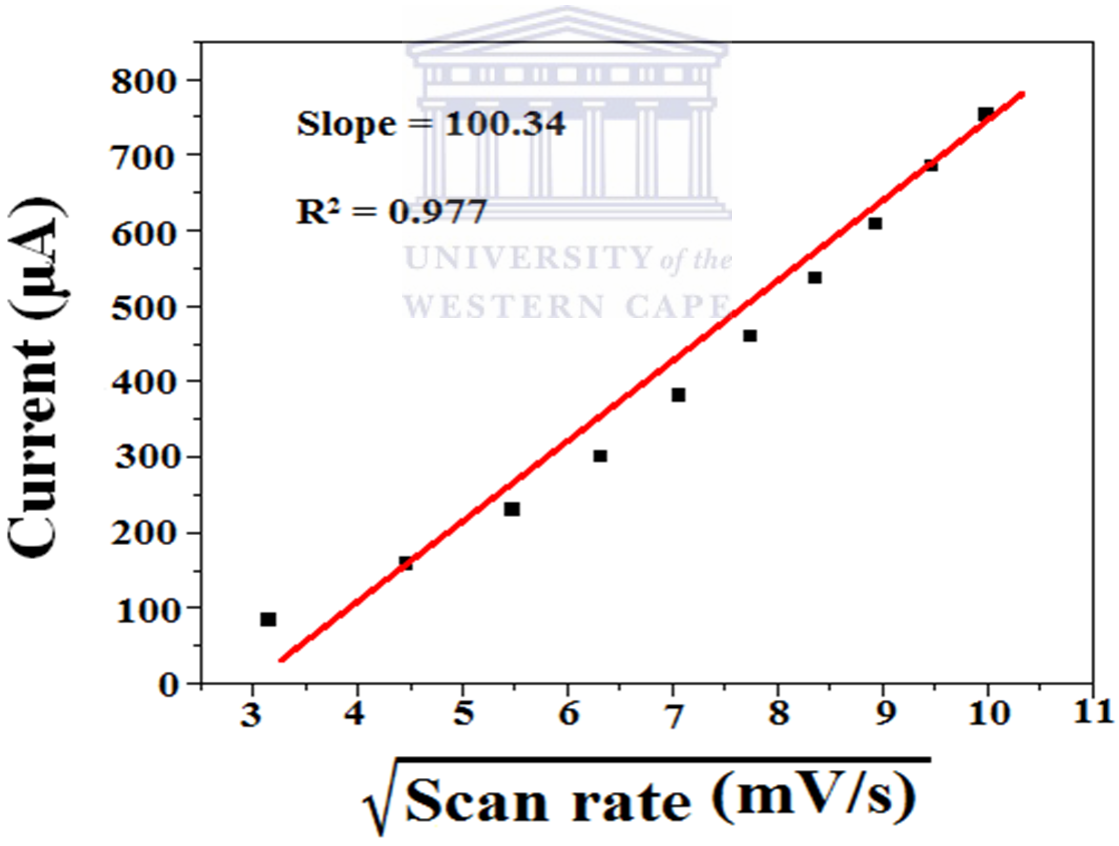

Figure 11: The Randles-Sevčik plot .of polypyrrole extrapolated from figure 10.

Figure 11shows the linear dependency of the current on the scan rate of the anodic peak B in figure 9. The Randles-Sevčik plot seems to indicate a thin surface bound electro-active polymer film. Furthermore the magnitude of the peak current was observed to increase with an increment of the scan rate suggesting that the peak current is diffusion controlled.

Randle Sevčik Plot given, for analysis of diffusion controlled reactions:

$$i_p = 0.0463nFA\left[\frac{nF}{RT}\right]C_0^* D_0{}^{1/2}\nu^{1/2} \qquad \text{Equation (3)}$$

Where I_p = (Peak Current in μA), n = 1 (number of electrons), F = 96485 C/mol (Faradays Constant), A = 0.0201 cm^2 (area of the electrode), C_0 * = mol/dm^2 (Concentration of bulk substrate concentration), R = 8.314 J mol/ K (Gas Constant), T = 298.15 K (absolute Temperature) and ν = (Scan Rate in V/s) and D_0 (diffusion co-efficient).

D_o is the electron charge transport coefficient sometimes also known as the rate of electron charge propagation along the polymer chain. Figure 9 indicates an oxidation reaction that was occurring at E_{pa} which was seen to be diffusion controlled with a correlation co-efficient of R^2 = 0.977 and a diffusion co-efficient of D_o = 3.4 X 10^{-8} cm^2/s; indicating a faster electron transfer kinetics within the diffusion layer. Figure 9 shows that the cathodic peak potentials of the polypyrrole at B', to overlap with an increase in scan rate suggesting a decrease in the rate of electron transfer.

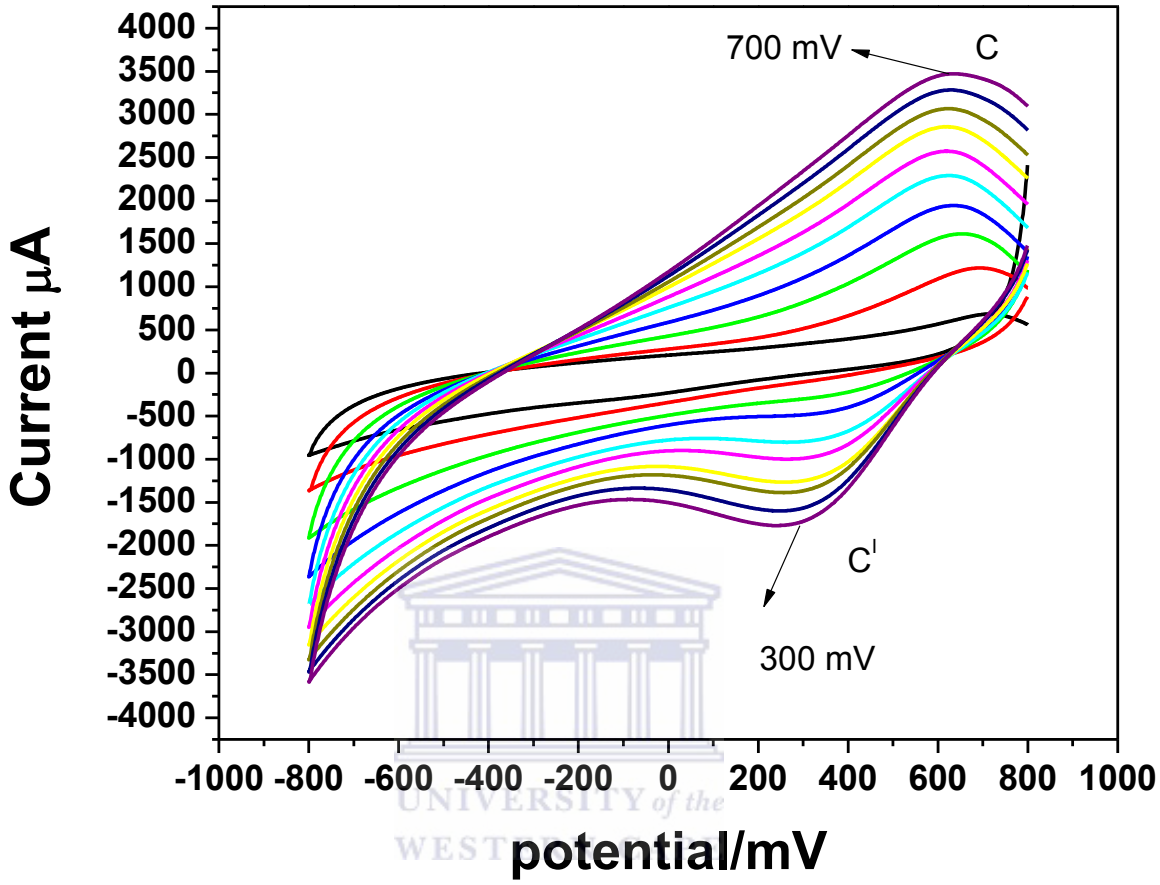

Figure 12: Cyclic Voltammogram of Ni-PPI-PPY star copolymer in 0.1 M phosphate buffer. Cyclic voltammogram was taken from scan rates of 10-100 mV/s, with 10 mV/s increments from -800 mV to +800 mV.

Figure 12 shows the cyclic voltammogram of Ni-PPI-PPY, with 2 observable peaks donated C and C^{l}. The oxidation state of the nickel in the complex was found to be +2. The number of electrons in the system were found to be n=1. ΔE_p [$E_{p,a} - E_{p,c}$] for the polymer film grown at different scan rates was calculated and found to be lower than 65mV. This suggested that the polymer exhibited reversible and fast electrochemistry. The cathodic peak at +300 mV, denoted as $C^{l,}$ is observed to be increasing with an increase in the scan rate. There is a slight cathodic shift in the peak potential; this is attributed to the extended conjugation in the polymer which results in the lowering of the oxidation

potential of the polymer. The anodic peak denoted by C, at 700mV is due to the change in the oxidation state of the nickel metal, this peak is represented by the mechanism Ni^{+}-- Ni^{2+} +e. There is no shift in this peak with an increase in scan rate, this indicates a surface bound species, and thus the Ni-PPI-Ppy star copolymer is a surface bound species.

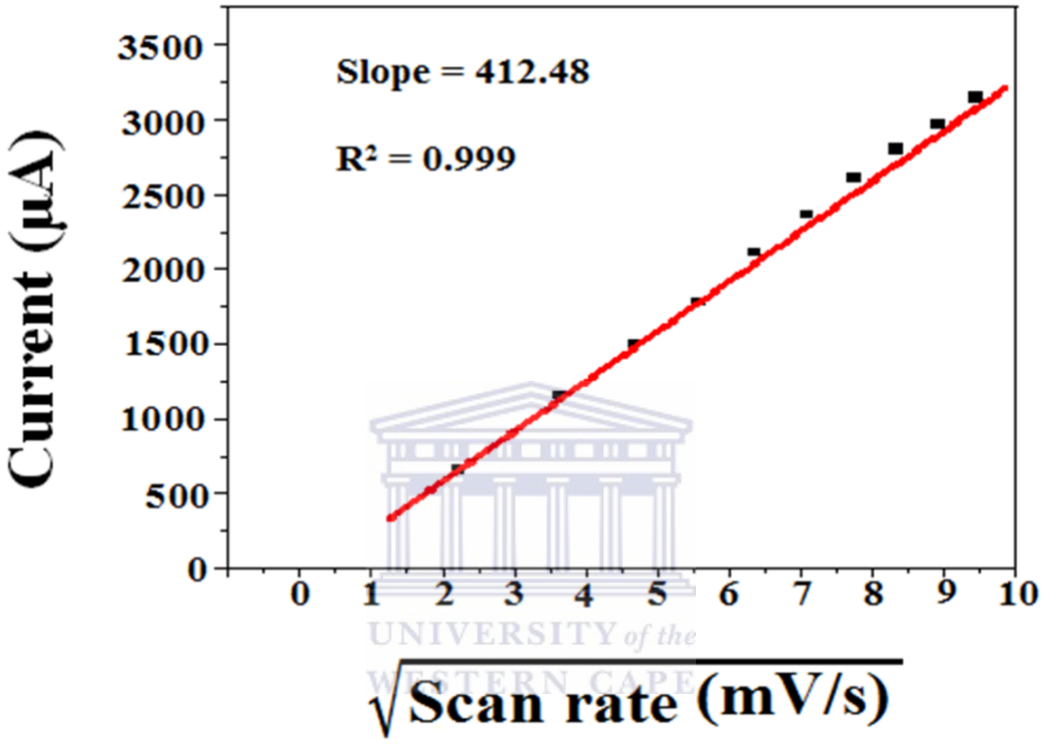

Figure 13: Randles-Sevčik plot of Ni-PPI-PPY star copolymer in 0.1 M phosphate buffer extrapolated from figure 12.

Figure 13 shows the e linear dependency of the current on the scan rate of the anodic peak C in figure 12. The Randles-Sevčik plot of Ni-PPI-PPY star copolymer indicates that the oxidation reaction occurring at E_{pa} was diffusion controlled with correlation co-efficient of r^2 = 0.999 and a diffusion co-efficient which was found to be D_o = 5.7 X 10^{-7} cm^2/s; indicating diffusion control and this was found to be higher than the diffusion coefficient calculated for polypyrrole (figure 10) which was found to be D_o = 3.4 X 10^{-8} cm^2/s. This

indicated that the Ni-PPI-PPY star copolymer increased the electron transfer, due to the increase in the conjugation of single (σ) and double (π) bonds, in the star copolymer due to the polymerization of polypyrrole and also the incorporation of the Ni metal into the framework of the star copolymer also plays a role in increasing the rate of electron movement in the star copolymer.

4.3. Biosensor characterization and detection of PZA

4.3.1. Electrochemistry of Ni-PPI-PPy/CYP2E1/BSA/Glu/Pt

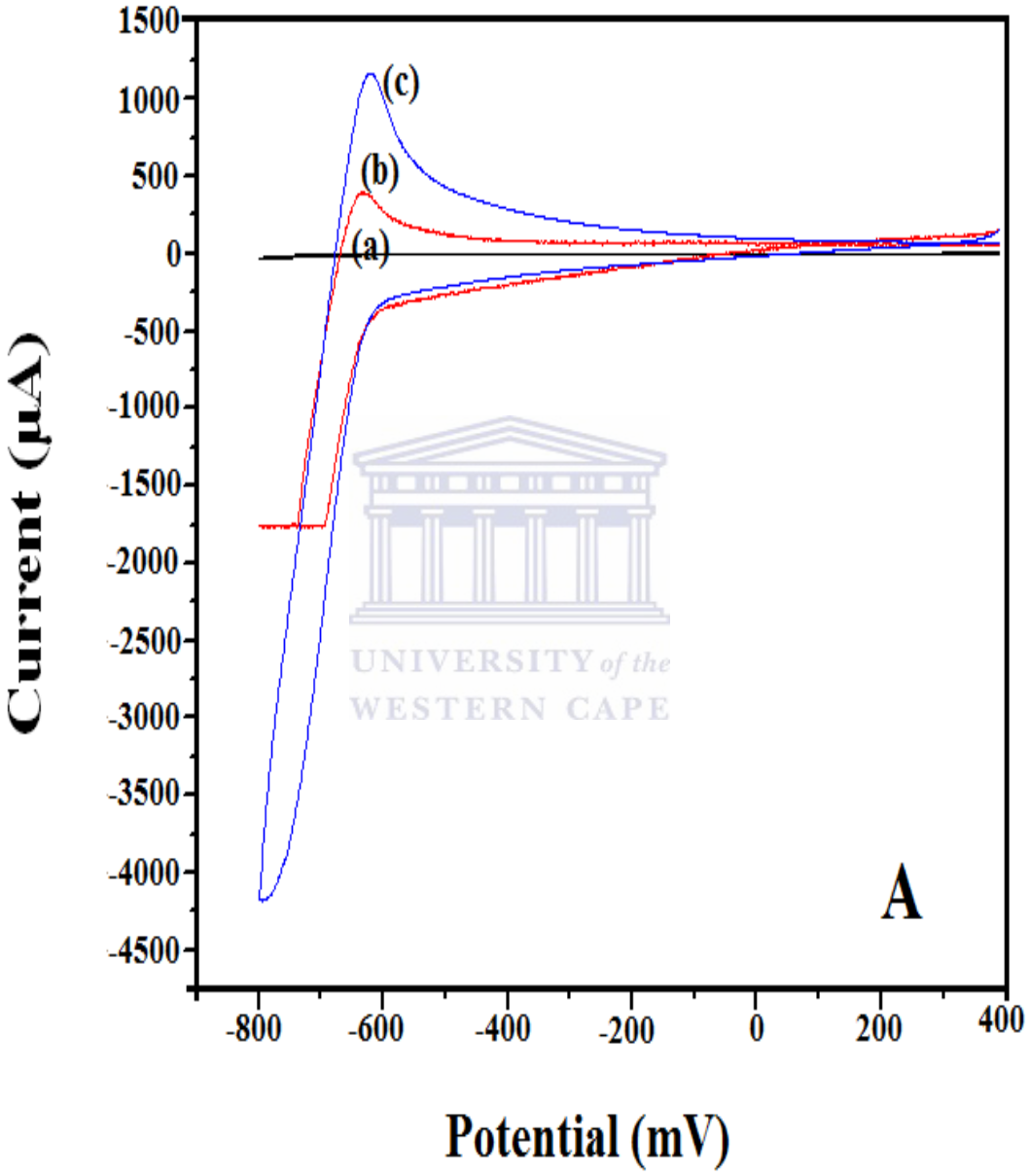

Figure 14: **(A)**. CV graph of (a) Ni-PPI-Ppy star copolymer/Pt, (b) CYP2E1/Pt and (c) Ni-PPI-Ppy star copolymer/CYP2E1/BSA/Glu/Pt nanobiosensor in 0.1 M phosphate buffer at 10 mV/s

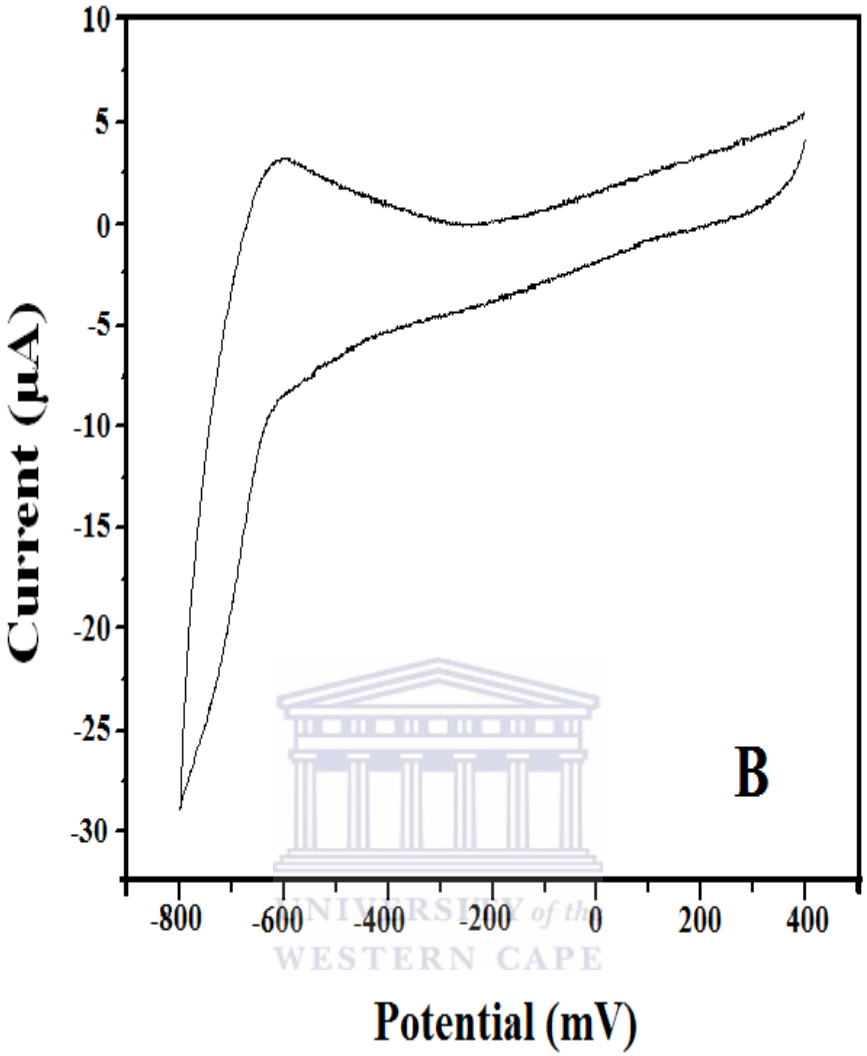

Figure 14:. **(B)** a magnified CV of the star copolymer.

Figure 14 shows the cyclic voltammograms of (a) Ni-PPI-Ppy star copolymer/Pt, (b) CYP2E1/Pt and (c) Ni-PPI-Ppy star copolymer/CYP2E1/BSA/Glu/Pt nanobiosensor in 0.1 M phosphate buffer at 10 mV/s. The current response increases when the enzyme is immobilized on the surface of the electrode. The voltammogram of the Ni-PPI-Ppy star copolymer/Pt shows the lowest current response and is marginalized when overlaid with CYP2E1/Pt and Ni-PPI-Ppy star copolymer/CYP2E1/BSA/Glu/Pt. The highest current

response is observed when the CYP2E1 enzyme is immobilized on top of the star copolymer.

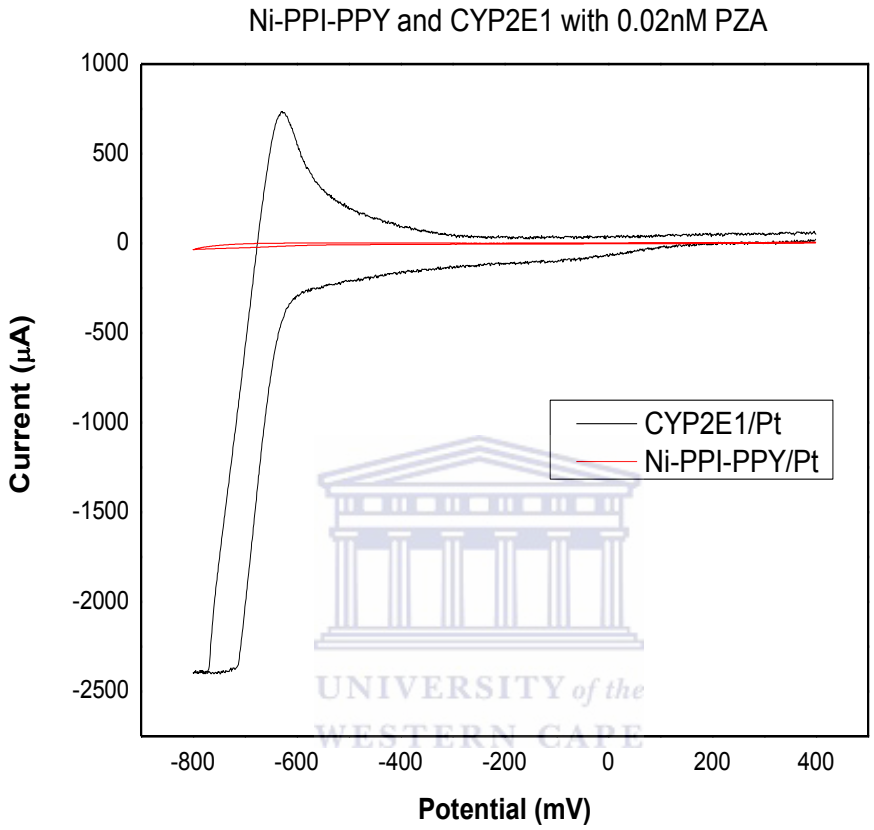

Figure 15: Cyclic voltammogram of Ni-PPI-PPY/Pt (red) and CYP2E1/Pt (black) (CYP2E1 enzyme on the surface of the bear Pt electrode) with 0.02 nM PZA in 0.1 phosphate buffer at a scan rate of 10 mV/s from -800 to 400 mV (vs. Ag/AgCl).

Figure 15 compares the response of the star copolymer and CYP2E1/Pt to the addition of PYZ concentrations. The voltammogram (**Figure 15**) is taken at a concentration 0.02nM PYZ, from the comparison it can be seen that the CYP2E1 gives a higher current response than the star copolymer, from that it can be seen that the enzyme is successfully

immobilized on the electrode and it metabolizes the PZA whereas the star copolymer gives minimal interaction as there is no enzyme to bind the PZA.

4.3.2. Detection of PZA

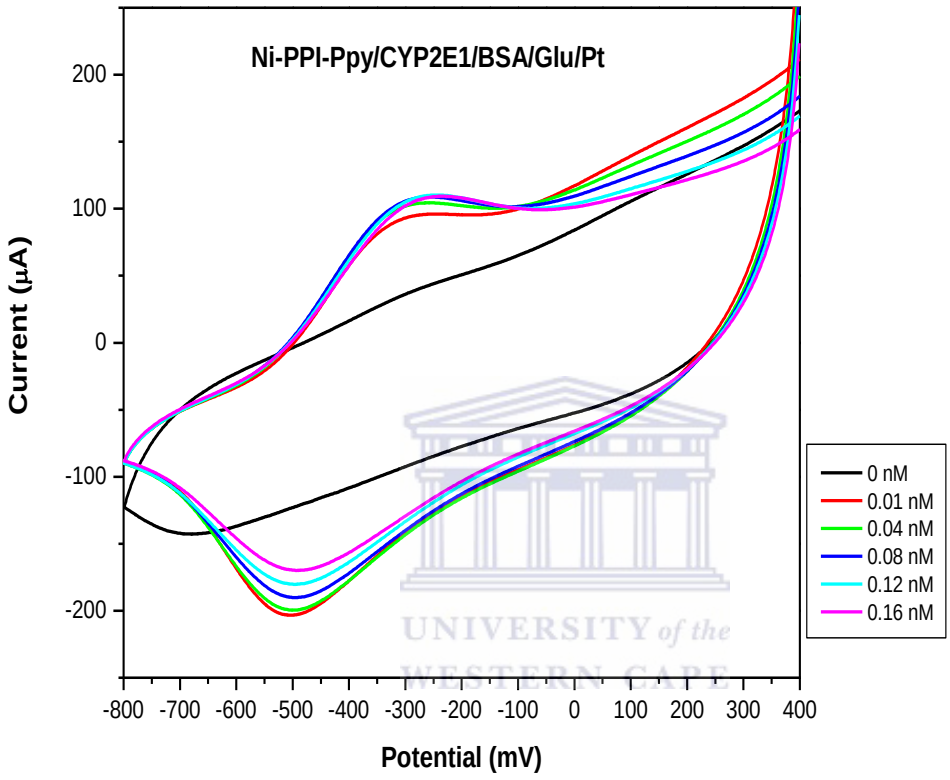

Figure 16: Cyclic Voltammogram of Ni-PPI-Ppy/CYP2E1/BSA/Glu/Pt with different concentrations of PZA in 0.1 phosphate buffer taken from -800 to 400 mV (vs. Ag/AgCl).

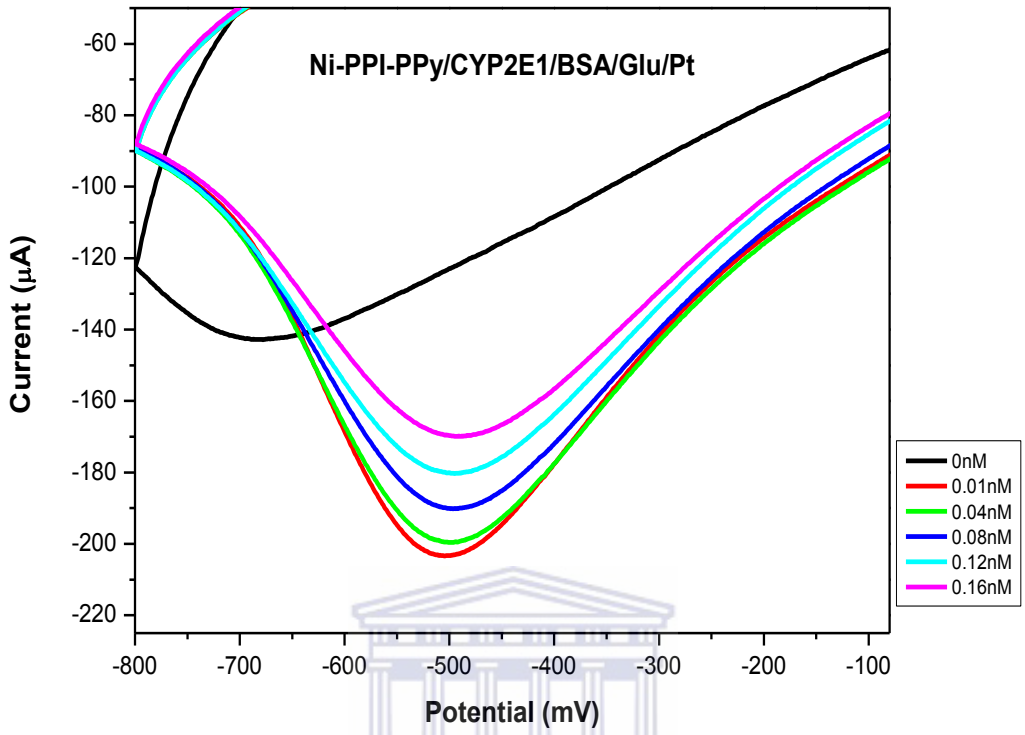

Figure 17: Cyclic Voltammogram of Ni-PPI-Ppy/CYP2E1/BSA/Glu/Pt with different concentrations of PZA in 0.1 phosphate buffer taken from -800 to -100 mV (vs. Ag/AgCl).

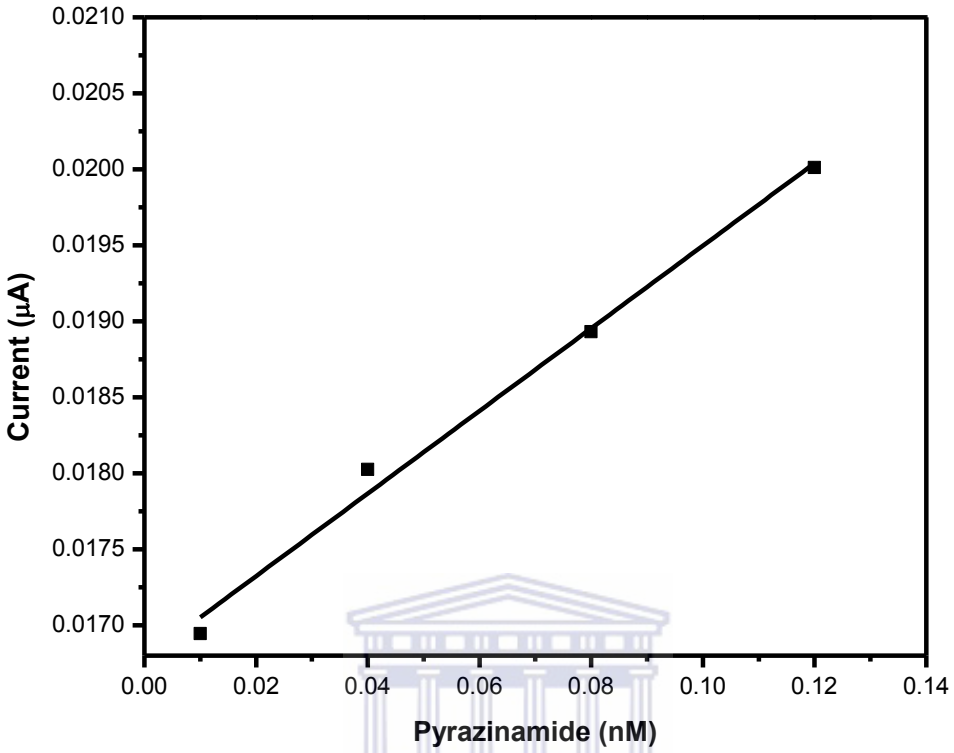

Figure 18: Calibration curve drawn from the linear region of the biosensor responses in figure 16.

The electrochemical activity of the CYP2E1 nanobiosensor (Ni-PPI-Ppy/CYP2E1/BSA/Glu/Pt) was evaluated using CV (**Figure 16**) in the presence of oxygen. From the CV it can be seen that the CYP2E1 nanobiosensor it exhibits one redox pair centred at -300 mV and -500 mV (vs. Ag/AgCl). This pair was attributed to the Fe^{3+}/Fe^{2+} transitions of the CYP2E1 active site. This suggests that the electron transfer that occurred at -300 mV (vs Ag/AgCl). The cathodic peak at -500 mV (vs Ag/AgCl) is indicative of the reduction of PZA-CYP2E1-O_2; this result is in agreement with the

mechanism for metabolic reaction of cytochrome P450 (haemolytic) enzymes (Scheme 3) **[32, 3]**. Thus, the -PPI-PPY star copolymer must have a great effect on the kinetics of electrode reaction providing a suitable environment for CYP2E1 to transfer electrons with the underlying electrode **[3]**.

The most important aspect of the study, detection of PZA, was interrogated using CV; figure 17 shows the reduction peak of the CYP2E1 nanobiosensor. The reduction peak was observed to increase with increase in the PZA concentration. This behaviour is attributed to the coupling of the fast electron transfer at the electrode surface with the reduction of PZA on or within the biosensor film **[3]**. The catalytic reduction mechanism of PZA by the biosensor is similar to the mechanism shown in scheme 3. The first step is the binding of PZA into the active site of CYP2E1 which is in the ferric resting state. An electron from the star copolymer modified electrode reduces the enzyme to the ferrous state which then binds to molecular oxygen. During this stage, PZA is hydroxylated to 5-hydroxypyrazinamide. This is followed by the O-O bond cleavage by the introduction of the second electron resulting in a highly active iron-oxoferryl intermediate CYP2E1 (Fe4+) with 5-hydroxypyrazinoic acid as the product which is released **[3]**.

The peak currents of the CYP2E1 nanobiosensor seen in figure 16, have a linear relationship with PZA concentrations, as shown in figure 18, with a dynamic linear range of 0.01 nM-0.12 nM (1.231 – 7.386 ng/L PZA) The developed nanobiosensor shows a higher sensitivity (0.142 µA/nM) and lower limit of detection (LOD) of pyrazinamide 0.00114 nM (0.14 ng/L) than that of chromatography at 500 mg of pyrazinamide is 40 ng/L **[52, 53-**

54]. This result shows that the biosensor is able to detect concentrations lower than that **[21]**. From The HPLC analysis of human blood, the peak concentration (C_{max}) of PZA determined 2 h after drug intake is 2.79 – 3.22 ng/L, which is very detectable with the nanobiosensor due to its high sensitivity **[52, 53- 54]**.

CHAPTER 5

5.1 Conclusion

Summary

This chapter covers the various aspects (success and challenges) towards the achievement of the main aims of the study. Where necessary, the chapter also entails future investigations and related studies.

This study has been conducted to develop a nanobiosensor for detection of an antituberculosis drug, pyrazinamide. The biosensor employed the heme enzyme, CYP2E1, immobilized onto a nickel-functionalized generation 2 poly(propylene imine) and polypyrrole star copolymer composite.

A star copolymer is a branched polymer molecule in which a single branch point gives rise to multiple linear chains or arms. Forming star copolymers increases the conductivity of polymers. Conducting polymers typically contain as the fundamental structural unit a linear backbone of repeating conjugated monomers, exemplified by polyacetylene, polypyrrole, polyaniline, and polythiophene. In this study polypyrrole was used as the repeating conjugated monomer. Organic conducting and semiconducting polymers may be synthetically tailored to optimize desirable properties such as melting point, melt viscosity, solubility, electrical and thermal conductivity. In general, conductive/semiconducting polymers consist of a backbone of repeating monomer units with extended pi-electron delocalization. In this project, the electrical conductivity of the conducting polymers was utilized in fabricating the biosensor. The nickel poly(propylene imine)-co-polypyrrole star copolymer was used as the platform of the biosensor to increase the electron movement between the analyte and the electrode. The nickel poly(propylene imine)-co- polypyrrole star co polymer was found to increase the conductivity of the biosensor by making use of its conjugation of single and double bonds, hic act as charge carriers.

SEM, TEM, EDS and FTIR studies showed successful incorporation of the nickel in the dendrimeric polymer with a change in morphology, crystal structure and new elements. The polymerization of the metallodendrimer with pyrrole, thus forming the star copolymer (Ni-PPI-PPY) resulted in a copolymer platform with improved electroactivity due to the incorporation of the Ni metal into the framework of the PPI dendrimer and the increase in single bond- double bond conjugation the electropolymerization of pyrrole on the Ni-PPI-2Py. This behaviour was investigated using CV where, after the formation of the star copolymer, the electroactivity was seen to improve due to the fact that electron transfer improved and peak currents increased. The CV results for the biosensor response towards different PZA concentrations confirmed that the Ni-PPI-Ppy/CYP2E1/BSA/Glu/Pt nanobiosensor successfully catalyzed the reduction of PZA into the main metabolite, pyrazinoic acid, well-known to destroy the TB bacteria. A calibration plot from the increasing PZA concentrations plotted against increasing currents was used to determine the sensitivity and limit of detection of the biosensor, which were found to be 0.142 µA/nM and 0.00114 nM (0.14 ng/L) respectively. The linear range was found to be 0.01 nM-0.12 nM (1.231 – 7.386 ng/L PZA).

Ngece and colleagues fabricated a nanoparticulate of silver-modified poly(8-anilino-1 naphthalene sulphonic acid) nanobiosensor systems for the determination of tuberculosis treatment drugs. Their biosensor was used to detect anti-Tuberculosis drugs, Isoniazid, Ethambutol, Rifampicin and Pyrazinamide. Using their biosensor to detect pyrazinamide, they found that the sensitivity of the -modified poly(8-anilino-1 naphthalene sulphonic acid) nanobiosensor system 1.38 µA/µM. The LOD and dynamic linear range were found to be 0.054µM and 0.054 µM-24 µM respectively.

Sidwaba and colleagues developed a nanobiosensor for detecting pyrazinamide, using PANI incorporated with multiwalled carbon nanotubes as the platform. They found that the sensitivity and limit of detection of the biosensor were found to be 0.959 µA/µM and 0.00916 µM (0.114 ng/L) respectively.

The cytochrome P4502E1/nickel-poly(propylene imine) dendrimeric nanobiosensor developed in this study is more sensitive than both biosensors, and can detect lower

concentrations than the two respective biosensors. The linear range of the cytochrome P4502E1/nickel-poly(propylene imine) dendrimeric nanobiosensor requires improvement.

Overall, the developed novel nanobiosensor showed catalytic response towards detection of pyrazinamide. The fundamental point is the detection limit of the nanobiosensor which falls within the C_{max} value of PZA determined by HPLC. Therefore, this compound is very detectable using this nanobiosensor. The biosensor is useful as it is more sensitive and is able to detect lower concentrations than other novel biosensors.

Recommendations for Future Study:

The following aspects of the nanobiosensors for the determination of Pyrazinamide, a first line tuberculosis treatment drug presented in this work warrant further investigations.

1. More work needs to be done to improve the electroactivity of PPI through the synthesis of higher generations.

2. It is proposed that another enzyme with a bigger active site than CYP2E1 that can metabolize Pyrazinamide be used, so that the sensitivity and linear range can be increased.

CHAPTER 6

Summary

This chapter gives a list of the consulted and quoted sources used throughout during reviewing of the study.

6.1. References

1. World Health Organization. 2014. *Global Tuberculosis report*, pp: 1-47.
2. USAID. 2010, "Treatment of Tuberculosis", *Tuberculosis Project South Africa* pp: 1-76.
3. U. Sidwaba. 2013, " Development of nano biosensors for phenolic endocrine disrupting compound and anti- Tuberculosis drug", *A thesis submitted in fulfilment of the requirements for degree in Masters Scientiae in Nano Science Faculty of Science University of Western Cape* (November2013).
4. R. Mackenzie. J. Voros. E. Reimhult. 2008, "Electrochemical biosensors- sensors principles of architectures", *Sensor*, 8, pp: 1400-1458 (2008) available [online] http://www.mdpi.org/sensors
5. A. Erdem. M. Bryszewska. 2002, "Electrochemical DNA biosensor based on DNA-Drug Interactions", *Electro-analysis*, 14, No.14, pp: 965-975.
6. Z. Zhao. H. Jiang. 2000, "Enzymes based on electrochemical Biosensors", *Electrochemical Biosensors*, pp: 1-23 available [online] http://www.intechopen.com

7. K. Arshak. V. Valusami. O. Luise. K. O. Stasiak. C. Adley. 2009, "Conducting polymers and their application to biosensors", *IEEE Sensor Journal*, 9, No. 12, pp: 1942-1952.

8. M. F. Suarez-Herrera. 1960, "Conducting Polymers", *Electrochemistry: University Nacional de Colombia, Bignonia, Colombia(Ed),* pp: 11-13

9. M. Y. Khuhawa. F. M. A.Rind. 2002, "Liquid chromatographic determination of isoniazid, pyrazinamide and rifampicin from pharmaceutical preparation and blood", *Journal of Chromatography* B, 766, pp: 357-363 available [online] http://www.elsivier.com/locate/chromb

10. http:www.storify.com/newtbdrugs/the-love-hate-relationship-with-pyrazinamide. [24 July 2014].

11. Yildiz Uludag, Biosensors 2010, 20th anniversary world congress on biosensors, Glasgow. http://www.yildizuludag.wordpress.com/category/biosensors [15 May 2014].

12. C. Li.2011, "Introduction and Overview of biosensors and electrochemistry." *Biosensors and Nano-Bioelectronics*, pp: 1-35 (2011).

13. M. Keusgen. 2002, "Biosensors: new approaches in drug discovery", *Naturwissenschaften,* Vol.83, pp: 433–444.

14. E. Galindo. 2000, Institute of Biotechnology National University of Mexico, Currence, Mexico", Biosensor. Vol. 11, pp: 1-9.

15. M. Gerald. A. Chanbey. B. D. Marhorta. 2002, "Application conducting polymers to biosensors", *Biosensors and Bioelectronics*, 17, pp: 345-359 available [online] http://www.elsevier.com/locate/boos.

16. B. Klajnert. M. Bryszewaka. 2001 "Dendrimers: Properties and applications", *Acta Biochemica Polonica*, 48, No 1/2001, pp: 199-208.

17. L. M. Cele. S. S. Ray. N. J. Conville.2009 "Nano science and nanotechnology in South Africa", *South African Journal of Science,* Vol.105, No.7/8, pp: 242 (July/August 2009) available [online] http://www.assaf.org.za

18. S. Brahim. A. M. Wilson. D. Narinesingh. E. Iwuoha. A. Guiseppi-Elie. **2003, "**Chemical and biological sensors based on electrochemical detection using conducting electroactive polymers", *Microchim. Acta,* 143, pp: 123–137 (2003).

19. D. T. Hoa. T. N. S. Kumar. N. S. Punekar. R. S. Srinivasa. R. Lal. A. Q. Contractor. 1992, "Biosensor based on conducting polymers" in *Analytical Chemistry*, 64, pp: 2645-2646 (1992).

20. M. H. Harun. E. Saion. A. Kassim. N. Yahya. E. Mahmud. 2007, "Conjugated Conducting Polymers: a brief overview", *JASA*, pp: 63-69.

21. K. Arshk. V. Velusamy. O. Korostynsk. K. Oliwa-Stasiak. C. Adley. 2009, "Conducting polymers and their applications to biosensors: emphasizing on foodborne pathogen detection", *IEEE SENSORS JOURNAL*, 9, NO. 12, pp: 1942-1952 (2009).

22. G. Smith. R. Chen. S. Mapolie. 2003, "The synthesis and catalytic activities of first generation poly(polypropylene immune) pyridylimine palladium metallodendrimers", *Journal of Organometallic Chemistry*, Vol.673, pp: 111-115 AVAILABLE [ONLINE] http://www.elsevier.com/locate/jorganchem

23. P. Holster. C. R. Van. T. Haeper. 2003, "Dendrimers", *Technology White Papers*, pp: 20-33 available [online]http://www.cientifica.com.

24. A. Pron. P. Rannou. 2002, "Processible conjugated polymers: from organic semi conducted metals and to organic superconductor", *Progress in Polymer Science*, Vol. 27, pp: 135-190 available [online]http://www.elsevier.com/locate/pplysci

25. A. Baleg. 2011, "Synthesis and Electrochemistry of novel conducting dendrimeric star copolymers on poly(propylene imine) dendrimer", *A thesis submitted in fulfilment of the requirements for the degree Doctor of Philosophy In Department of Chemistry, University of the Western Cape*, pp: 1-153.

26. N. C. Antonels. B. Therrienb. J. R. Mossa,. G. S. Smitha. 2009, "Rhodium (I) iminophosphine poly(propyleneimine) dendrimers: synthesis, characterization and molecular structure of a mononuclear analogue", *Inorganic Chemistry Communications,*Vol.12, issue 8, pp: 716-719.

27. D. Wang. T. Imae. M. Miki. 2007, "Fluorescence emission PAMAM and PPI dendrimers", *Journal of Colloid and Interface Science,* Vol.306, pp: 222-227 available [online] http://www.elsevier.com/locate/jcsi.

28. S.P. Malinga. O. A. Arotiba. R. W. Krause. S.F. Mapolie. B. Mamba. 2011, "Synthesis and characterization of generations 2 and 3 poly (polypropylene imine) dendrimer capped NIFE", *Material Letters,* pp: 440-555 available [online] http://www.elsevier.com/locate/mattlet.

29. N. Antonels. 2010, "Synthesis and characterization of poly(propyleneimine)-based rhodium(i) metallodendrimers and their evaluation as hydroformylation catalysts", *A thesis submitted to the University of Cape Town, fulfilment of the requirements for the degree of Master of Science,* pp: 1-88.

30. R. M. Enus. S. F. Mapolie. G. S. Smith. 2008 "Norbornene polymerization using multinuclear nickel catalyst based on a polypropylene imine dendrite scaffold", *Journal of Organometallic Chemistry,* 693, pp: 2279-2288 (2008) available [online] http://www.elsevier.com/locate/jotganchem.

31. R. Patrick .K. Porubsky. M. Merely. 2008, "Both small molecular weight and fatty acid insights into the binding of inhibitors and Structures of human cytochrome P450 2E1: substrates", J*ournal of Biological Chemistry*, pp: 3-22.

32. R. F. Ngece. 2011 "Nanoparticulate of silver- modified poly(8-anilino-1-naphthalene sulphonic acid) nanobiosensor system for the determination of Tuberculosis treatment drug" in *A thesis submitted in fulfilment of requirement for degree in Philosophiae, Chemistry Faculty of Science University of Western Cape*), pp: 1-194(June 2011).

33. V. V. Shumyatseva. T. V. Bulko. A. I. Archakov. 2005, "Electrochemical reduction of cytochrome P450 as an approach to the construction of biosensor and bioreactors", *Journal of Inorganic Biochemistry*, Vol. 99, pp: 1051-1063 (2005), available [online] http://www.elsevier.com/locate/ica.

34. N. Bistolas. U. Wollenberger. C. Jung. F.W. Scheller. 2005, "Cytochrome P450 biosensor-a review", *Biosensors Bioelectronics*. 20, pp: 2408-2423 (2005) available [online] http://www.sciencedirect.com.

35. E. Schneide. D. S. Clark. 2013, "Cytochrome P450 (CYP) enzymes and development of CYP biosensor", *Biosensors and Bioelectronics,* 39, pp: 1-13 available [online]http://www.elsevier.com/locate/bios

36. P. Panicco. V. R .Dodhia. A. Fantuzzi. G. Gilardi. 2011, "Enzyme-based amperometric platform to determine the polymorphic response in drug metabolism by cytochrome P450", *Analytical Chemistr*, 83, pp: 2179–2186 (2011) available [online] http://www. dx.doi.org/10.1021/ac200119b.

37. N. Bistolas. U. Wollenberger. C. Jung. F.W. Scheller. 2005, "Cytochrome P450 biosensor-a review", *Biosensors Bioelectronics*. 20, pp: 2408-2423 (2005) available [online] http://www.sciencedirect.com.

38. A. I. Cedelbaum.2004, "Cytochrome P450 polymorphism and drug metabolism" in *Pharmacogenetics course spring*, 25, No.4, pp: 193-200.

39. J.C. Helfrick Jr., L.A. Bottomley., 'Cyclic square wave voltammetry of single and consecutive reversible electron transfer reactions'. *Analytical Chemistry* 2009, 81, pp: 9041–9047.

40. Y. Zhu. H. Zhu. X. Yang. L. Xu. C. Li.2006, "Sensitive biosensors based on (dendrimer encapsulated pt nanoparticles)/enzyme multilayers", *Electro analysis*, 19, No. 6, pp: 698–703 (2006).

41. S. F. Douman. 2013, "The response of indium telluride quantum dots impedimenta genosensor for telomerase cancer in biomarker", *A thesis submitted in fulfilment of the*

requirements for degree in Masters Scientiae in Chemistry Faculty of Science University of Western Cape, pp: 1-7 (November 2013).

42. U. Feleni.2013, "Palladium telluride quantum dots biosensor for the determination of indinavir drug", *A thesis submitted in partial fulfilment of the requirements for the degree of Master Scientiae in Nano Science Faculty of Science University Of Western Cape*, pp: 1-113 (November 2013).

43. *http://www4.nau.edu/microanalysis/microprobe-sem/instrumentation.html*. [20 May 2014]

44. Joseph Goldstein. 2003. *Scanning Electron Microscopy and X-Ray* Microanalysis. *Springer*. *ISBN*, 978-0-306-47292-3.

45. U. B. Annika. J. Karlsson. B. F. M. de Waal. E. W. Meijer. 2001, "synthesis and properties of new thiourea-functionalized poly(propylene imine) dendrimers and their role as hosts for urea functionalized guests", *Journal of Organic Chemistry*, Vol.66, pp: 2136-2145 (2001).

46. G. R. Newkome. E. He. C. N. Moorefield. 1999, "Suprasupermolecules with novel properties: metallodendrimers", *Chemical Review*. 99, No.7, pp: 1689-1746 (1999).

47. K.D., Vernon-Parry, 'Scanning electron microscopy: an introduction'. Ill-Vs Review2000, 13, pp: 40-44.

48. F.M. Olid. E. de Jesus. J.C. Flores. 2014, "Monometallic nickel (II) complexes containing N, N-iminopryide chelating ligands with dendrite on catalytic oligomerization and polymerization of ethylene", *Inorganica Chimica Acta,* 409, pp: 156-163 available [online] http://www.elsevier.com/locate/ica.

49. V.A. Yazerski. R. J.M. K. Gebbink .2010. *Heterogenization of Homogeneous Catalysts on Dendrimers*. Chapter 5, Pp: 171-201 (2010).

50. J. M. Ramosa, M. deM. C. Anilton .C.C. J. Versianeb, C. A.T´ellezSotoa. 2011, "Fourier transform infrared spectrum: vibration assignments using density functional theory and natural bond orbital analysis of the bis (guanidoacetate) nickel (II) complex", *Science Asia,* 37, pp: 247-255 available [online] http://www.scienceasia.org.

51. A. H. Dawood. R. Khalaf, Z. Salman. 2009, "Cobalt(II), nickel(ii), and copper(ii) complexes with ligands contain nitrogen as donor atoms type n3 and azamacrocylic n6, synthesis and characterization", *National Journal of Chemistry*. 35, Pp: 489-505.

52. C. C. Boehme. M. D. Nabethe. M. D. D. Hillenemn. 2010 “Rapid molecular detection of Tuberculosis and rifampin resistance”, *The New England Journal of Medicine*, 363, No.11, pp: 1005-1016.

53. C. Marzolini. A. Telent. T. Buclin. J. Biollaz. L. A. Decosterd. 2000 “Simultaneous determination of HIV protease inhibitors indinavir, amprenavir, saquinavir, ritonavir, nelfnavir, and the non- nucleoside reverse transcriptase inhibitor efavirenz by high – performance liquid chromatography after solid phase extraction”, *Journal of Chromatography* B, 740, PP: 43-58 (2008) Available [online] http://www.elsevier.com/locate/chromb.

54. R. Panchagnude. A. Sood. M. Sharda. 1999, “Determination of rifampicin and its main metabolite in plasma and urine presence of pyrazinade and isoniazid by HPLC method”, *Journal of Pharmaceutical and Biomedical Analysis*. 18, pp: 1013-1020 (1999).